Evaluation of lipid biomarkers as proxies for sea ice and ocean temperatures along the Antarctic continental margin

Nele Lamping[1], Juliane Müller[1,2,3], Jens Hefter[1], Gesine Mollenhauer[1,2,3], Christian Haas[1], Xiaoxu Shi[1], Maria-Elena Vorrath[1], Gerrit Lohmann[1,3,4], Claus-Dieter Hillenbrand[5]

[1]Alfred Wegener Institute, Helmholtz Center for Polar and Marine Research, Am Alten Hafen 26, 27568 Bremerhaven, Germany

[2]Department of Geosciences, University of Bremen, Klagenfurter Straße, 28359 Bremen, Germany

[3]Marum - Center for Marine Environmental Sciences, Leobener Straße 8, 28359 Bremen, Germany

[4]Department of Environmental Physics, University of Bremen, 28359 Bremen, Germany

[5]British Antarctic Survey, High Cross, Madingley Road, Cambridge CB3 0ET, United Kingdom

Correspondence to: Nele Lamping (nele.lamping@awi.de)

Abstract

The importance of Antarctic sea ice and Southern Ocean warming has come into the focus of polar research during the last couple of decades. Especially around West Antarctica, where warm water masses approach the continent and where sea ice has declined, the distribution and evolution of sea ice play a critical role for the stability of nearby ice shelves. Organic geochemical analyses of marine seafloor surface sediments from the Antarctic continental margin allow an evaluation of the applicability of biomarker-based sea ice and ocean temperature reconstructions in these climatically sensitive areas. We analysed highly branched isoprenoids (HBIs), such as the sea-ice proxy $IPSO_{25}$ and phytoplankton-derived HBI-trienes, but also phytosterols and isoprenoidal glycerol dialkyl glycerol tetraethers (GDGTs), which are established tools for the assessment of primary productivity and ocean temperatures, respectively. The combination of $IPSO_{25}$ with a phytoplankton marker (*i.e.* the $PIPSO_{25}$ index) permits semi-quantitative sea-ice reconstructions and avoids misleading over- or underestimations of sea-ice cover. Comparisons of the $PIPSO_{25}$-based sea-ice distribution patterns and TEX^{L}_{86}- and RI-OH'-derived ocean temperatures with (1) sea-ice concentrations obtained from satellite observations and (2) instrument measurements of sea surface and subsurface temperatures corroborate the general capability of these proxies to determine oceanic key variables properly. This is further supported by model data. We also highlight specific aspects and limitations that need to be taken into account for the interpretation of such biomarker data and discuss the potential of $IPSO_{25}$ as an indicator for the former occurrence of platelet ice and/or the export of ice shelf water.

1. Introduction

One of the key components of the global climate system, influencing major atmospheric and oceanic processes, is floating on the ocean's surface at high latitudes – sea ice (Thomas, 2017). Southern Ocean sea ice is one of the most strongly changing features of the Earth's surface as it experiences considerable seasonal variabilities with sea-ice extent decreasing from a maximum of 20×10^6 km^2 in September to a minimum of 4×10^6 km^2 in March (Arrigo et al., 1997; Zwally, 1983). This seasonal waxing and waning of sea ice substantially modifies deep-water formation, influences the ocean-atmosphere exchange of heat and gas and strongly affects surface albedo and radiation budgets (Abernathey et al., 2016; Nicholls et al., 2009; Turner et al., 2017). Moreover, sea ice regulates ocean buoyancy flux, upwelling and primary production (Schofield et al., 2018).

Based on the 40-year satellite record, Southern Ocean sea-ice extent as a whole followed an increasing trend (Comiso et al., 2017; Parkinson and Cavalieri, 2012), experiencing an abrupt reversal from ca. 2015 to 2018 (Parkinson, 2019; Turner et al., 2020; Wang et al., 2019), which has been attributed to a decades-long oceanic warming and increased advection of atmospheric heat (Eayrs et al., 2021). However, the sea-ice extent around major parts of West Antarctica has been decreasing over the last 40 years (Parkinson and Cavalieri, 2012). The Antarctic Peninsula is particularly affected by a significant reduction in sea-ice extent and rapid atmospheric and oceanic warming (Etourneau et al., 2019; Li et al., 2014; Massom et al., 2018; Vaughan et al., 2003). The Larsen A and B ice shelves on the east coast of the Antarctic Peninsula collapsed in 1995 and 2002, respectively. These collapses were triggered by the loss of a sea-ice buffer, which enabled an increased flexure of the ice-shelf margins by ocean swell (Massom et al., 2018). Along the Pacific margin of West Antarctica, the Amundsen and Bellingshausen seas have also been affected by major sea-ice decline and regional surface ocean warming (Hobbs et al., 2016; Parkinson, 2019). Marine-terminating glaciers draining into the Amundsen and Bellingshausen seas are thinning at an alarming rate, which has been linked to sub-ice shelf melting caused by relatively warm Circumpolar Deep Water (CDW) incursions into sub-ice shelf cavities (e.g., Jacobs et al., 2011; Khazendar et al., 2016; Nakayama et al., 2018; Rignot et al., 2019; Smith et al., 2017). The disintegration of ice shelves reduces the buttressing effect that they exert on ice grounded further upstream, which can lead to partial or total loss of the ice in the catchments of the affected glaciers and, thus, raise global sea level considerably (3.4 to 4.4 m in case of a total West Antarctic Ice Sheet collapse; Fretwell et al., 2013; Jenkins et al., 2018; Pritchard et al., 2012; Vaughan, 2008).

State-of-the-art climate models are not yet fully able to depict sea-ice seasonality and sea-ice cover, which the 5th Assessment Report of the Intergovernmental Panel on Climate Change (Stocker et al., 2013) attributes to a lack of validation efforts using proxy-based sea-ice reconstructions. Knowledge about (paleo-)sea-ice conditions and ocean temperatures in the climate sensitive areas around the West Antarctic Ice Sheet is hence considered as crucial for understanding past and future climate evolution. To date, the most common proxy-based sea-ice reconstructions in the Southern Ocean utilize fossil assemblages of sympagic (i.e. living within sea ice) diatoms preserved within the seafloor sediments (Allen et al., 2011; Armand and Leventer, 2003; Crosta et al., 1998; Esper and Gersonde, 2014; Gersonde and Zielinski, 2000; Leventer, 1998). Dissolution effects within the water column or after deposition, however, determine the preservation of small, lightly silicified diatom taxa and therefore can alter the assemblage record, leading to inaccurate sea-ice reconstructions (Leventer, 1998; Zielinski et al., 1998). Recently, the molecular remains of certain diatom taxa, i.e. specific organic geochemical lipids, have emerged as a potential proxy for reconstructing past Antarctic sea-ice cover (Barbara et al., 2013; Collins et al., 2013; Crosta et al., 2021; Denis et al., 2010; Etourneau et al., 2013; Lamping et al., 2020; Massé et al., 2011; Vorrath et al., 2019; 2020). Specifically, a di-unsaturated highly branched isoprenoid (HBI) alkene (HBI diene, $C_{25:2}$) has been detected in both sea-ice diatoms from the Southern Ocean and Antarctic marine sediments (Johns et al., 1999; Massé et al., 2011; Nichols et al., 1988). Recently, the sympagic diatom *Berkeleya adeliensis*, which preferably proliferates in platelet ice, has been identified as the producer of these HBI alkene (Belt et al., 2016; Riaux-Gobin and Poulin, 2004). However, *B. adeliensis* seems rather flexible concerning its habitat, since it was also recorded in the bottom ice layer and is apparently well adapted to changes in texture during ice melt (Riaux-Gobin et al., 2013). Belt et al. (2016) introduced the term IPSO$_{25}$ ("Ice Proxy of the Southern Ocean with 25 carbon atoms") by analogy to the counterpart IP$_{25}$ in the Arctic. Commonly, for a more detailed assessment of sea-ice conditions, IP$_{25}$ in the Arctic Ocean and IPSO$_{25}$ in the Southern Ocean have been measured alongside complementary phytoplankton-derived lipids, such as sterols and/or HBI-trienes, which are indicative of open-water conditions (Belt and Müller, 2013; Lamping et al., 2020; Etourneau

91 et al., 2013; Vorrath et al., 2019; 2020). The combination of the sea-ice biomarker and a phytoplankton

92 biomarker, the so-called PIPSO$_{25}$ index (Vorrath et al., 2019), allows for a more quantitative

93 differentiation of contrasting sea-ice settings and helps to avoid misinterpretations of the absence of

94 IPSO$_{25}$. An absence of the sea-ice biomarker can result from either a lack of sea-ice cover or a permanent

95 thick sea-ice cover that prevents light penetration and hence limits ice algae growth. These two

96 contrasting scenarios can be distinguished by using the additional phytoplankton biomarker. Recently,

97 Lamping et al. (2020) used the PIPSO$_{25}$ index to reconstruct changes in sea-ice conditions during the

98 last deglaciation of the Amundsen Sea shelf, which were likely linked to advance and retreat phases of

99 the Getz Ice Shelf.

100 Multiple mechanisms exist that can cause ice-shelf instability. As previously mentioned, relatively

101 warm CDW is considered one of the main drivers for ice-shelf thinning in the Amundsen Sea and

102 Bellingshausen Sea sectors of the West Antarctic Ice Sheet (Nakayama et al., 2018; Jenkins and Jacobs,

103 2008; Rignot et al., 2019). Accordingly, changing ocean temperatures are another crucial factor for the

104 stability of the marine-based ice streams draining most of the West Antarctic Ice Sheet (e.g., Colleoni

105 et al., 2018). As for sea-ice reconstructions, organic geochemical lipid proxies have been employed

106 over the past decades for reconstructing ocean temperatures in high latitudes, since the abundance and

107 preservation of calcareous microfossils commonly used for such reconstructions is very poor in polar

108 marine sediments (e.g., Zamelczyk et al., 2012). In contrast, archaeal isoprenoidal glycerol dialkyl

109 glycerol tetraethers (isoGDGTs), sensitive to temperature change and relatively resistant to degradation

110 processes, are well preserved in all types of marine sediments (Huguet et al., 2008; Schouten et al.,

111 2013). Schouten et al. (2002) found that the number of rings in sedimentary GDGTs is correlated with

112 surface water temperatures and developed the first archaeal lipid paleothermometer TEX$_{86}$, a ratio of

113 certain GDGTs, as a sea surface temperature (SST) proxy. For polar oceans, Kim et al. (2010) developed

114 a more specific calibration model for temperatures below 15 °C, TEX$^{L}_{86}$, which employs a different

115 GDGT combination. There is an emerging consensus that GDGTs predominantly reflect subsurface

116 ocean temperatures (SOT) along the Antarctic margin (Kim et al., 2012; Etourneau et al., 2019; Liu et

117 al., 2020). This is supported by observations of elevated archaeal abundances (and GDGTs) in warmer

118 subsurface waters (Liu et al., 2020; Spencer-Jones et al., 2021). Archaea adapt their membrane in cold

119 waters by adding hydroxyl groups and changing the number of rings, OH-GDGTs (Fietz et al., 2020).

120 Huguet et al. (2017) found in molecular dynamic simulations that the additional hydroxyl moieties lead

121 to an increase of the membrane fluidity, which aids trans-membrane transport in cold environments.

122 This explains the higher relative abundance of OH Archaea lipids in cold environments. Taking the

123 OH-GDGTs into account, Lü et al. (2015) proposed an SST-proxy for the polar oceans, the RI-OH'.

124 The aim of our study is to provide insight into the application of biomarkers in Southern Ocean

125 sediments as sea ice and ocean temperature proxies. Estimates on recent sea-ice coverage and ocean

126 temperatures along the eastern and western Antarctic Peninsula (EAP and WAP) as well as in the

127 Amundsen and Weddell seas are based on the analyses of IPSO$_{25}$, HBI-trienes and phytosterols and

128 GDGTs in seafloor surface sediment samples from these areas. A comparison of biomarker-derived

129 estimates of sea-ice extent and ocean temperature with (1) sea-ice distributions obtained from satellite

130 observations and (2) in-situ ocean temperature measurements allows for an evaluation of the proxy

131 approach. We further consider AWI-ESM2 climate model data to assess the model's performance in

132 depicting recent oceanic key variables and to examine the potential impact of paleoclimate conditions

133 on the biomarker composition of the investigated surface sediments. Taking into account the various

134 factors affecting the use of marine biomarkers as paleoenvironmental proxies, we comment on the

135 limitations of GDGT temperature estimates and the novel PIPSO$_{25}$ approach. Furthermore, we discuss

136 the potential connection between IPSO$_{25}$ and platelet ice formation under near-coastal fast ice, which is

137 related to the near-surface presence of sub-ice shelf melt water.

138

139 **2. Regional setting**

140 The areas investigated in this study include the southern Drake Passage, the continental shelves of the

141 WAP and EAP (~60° S) and the more southerly located Amundsen and Weddell seas (~75° S; Fig. 1).

142 The different study areas are all connected by the Antarctic Circumpolar Current (ACC), the Antarctic

143 Coastal Current and the Weddell Gyre, respectively (Meredith et al., 2011; Rintoul et al., 2001).
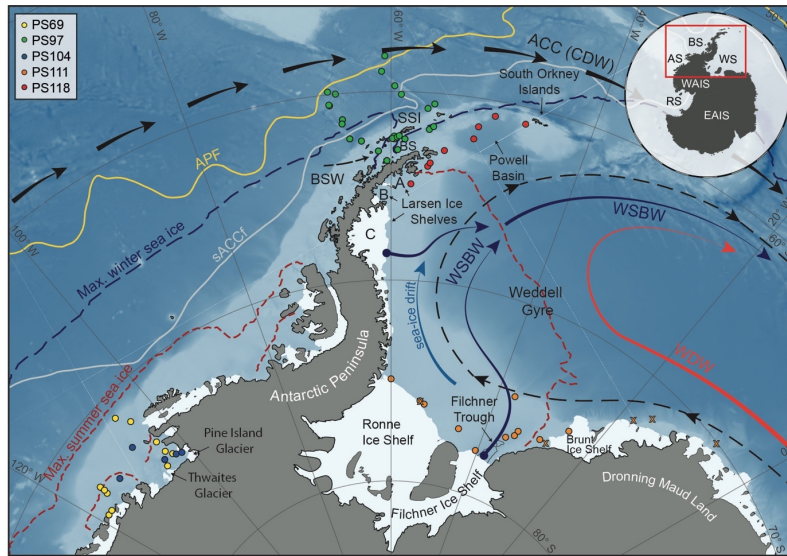
Fig. 1: Map of the study area (location indicated by red box in insert map) including all 41 sample locations (see different colored dots for individual RV *Polarstern* expeditions in the top left corner; for detailed sample information, see Table S1) and main oceanographic features. Maximum summer and winter sea-ice boundaries are marked by dashed red and blue line, respectively (Fetterer et al., 2016). The orange crosses in the Weddell Sea indicate samples with low biomarker concentrations close to detection limit, to which we assigned a PIPSO$_{25}$ value of 1. ACC: Antarctic Circumpolar Current, APF: Antarctic Polar Front, sACCf: southern Antarctic Circumpolar Current Front, SSI: South Shetland Islands, BS: Bransfield Strait, BSW: Bellingshausen Sea Water, CDW: Circumpolar Deep Water, WDW: Weddell Deep Water, WSBW: Weddell Sea Bottom Water (Mathiot et al., 2011; Orsi et al., 1995). Insert map shows grounded ice (*i.e.* without ice shelves) in black; WAIS: West Antarctic Ice Sheet, EAIS: East Antarctic Ice Sheet, RS: Ross Sea, AS: Amundsen Sea, BS: Bellingshausen Sea, WS: Weddell Sea. Background bathymetry derived from IBCSO data (Arndt et al., 2013).

144   The ACC, which is mainly composed of CDW and characterised by strong eastward flow, is the largest

145   current system in the world and has its narrowest constriction in the Drake Passage. In the Amundsen

146   Sea, the Bellingshausen Sea and along the WAP, where the ACC flows close to the continental shelf

147   edge, CDW is upwelling onto the shelf and flows to the coast via bathymetric troughs, contributing to

148   basal melt and retreat of marine-terminating glaciers and ice shelves (Cook et al., 2016; Jacobs et al.,

149   2011; Jenkins and Jacobs, 2008; Klinck et al., 2004). In the Weddell Sea, the Weddell Gyre, a subpolar

150   cyclonic circulation south of the ACC, deflects part of the ACC's CDW towards the south and turns it

151   into Warm Deep Water (WDW; Fig. 1; Hellmer et al., 2016; Vernet et al., 2019). In close vicinity to

152   the Filchner-Ronne and Larsen Ice Shelves, glacial meltwater as well as dense brines released during

153   sea-ice formation contribute to the formation of Weddell Sea Bottom Water (WSBW) - a major

154   precursor of Antarctic Bottom Water (Hellmer et al., 2016). Along the EAP coast wind and currents

155   force a northward drift of sea ice (Harms et al., 2001), which melts when reaching warmer waters in the

156   North and in Powell Basin (Vernet et al., 2019). At the northern tip of the Antarctic Peninsula, colder

157   and saltier Weddell Sea water masses branch off westwards into the Bransfield Strait, where they

158   encounter the well-stratified, warm, and fresh Bellingshausen Sea Water (BSW; Fig. 1), which is

159   entering the Bransfield Strait from the West (Sangrà et al., 2011).

160   Since 1978, satellite observations show strong seasonal and decadal changes in sea-ice cover around

161   the Antarctic Peninsula, which are less pronounced in the Amundsen and Weddell seas (Vaughan et al.,

162   2003; Parkinson and Cavalieri, 2012). Mean monthly sea-ice concentrations (SIC) for austral winter

163   (JJA), spring (SON) and summer (DJF) reveal a permanently ice-free Drake Passage, while the WAP

164   and EAP shelf areas are influenced by a changing sea-ice cover throughout the year (Fig. 2a-c). For the

165   Amundsen and Weddell seas, satellite data reveal up to ~90 % sea-ice concentration during winter and

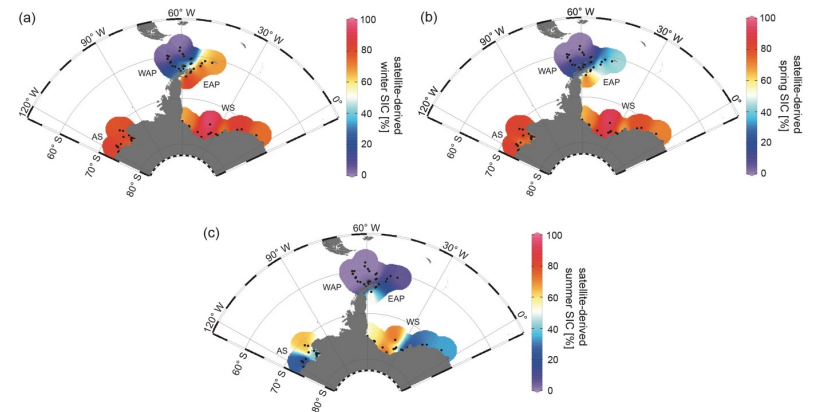166   spring (Fig. 2a+b), and a minimum concentration of ~30 % during summer (Fig. 2c).

Fig. 2: Distribution of mean monthly satellite-derived sea-ice concentrations for (a) winter (JJA), (b) spring (SON) and (c) summer (DJF) in % (downloaded from the National Snow and Ice Data Center, NSIDC; Cavalieri et al., 1996). AS: Amundsen Sea, WAP: West Antarctic Peninsula, EAP: East Antarctic Peninsula, WS: Weddell Sea.

3. Material and methods

3.1 Sediment samples

We analysed a set of 41 surface sediment samples (0-1 cm subbottom depth) from different areas of the Southern Ocean (Fig. 1) retrieved by multicorers and giant box corers during RV *Polarstern* expeditions over the past 15 years. Sixteen surface sediment samples from the Amundsen Sea continental shelf were collected during expeditions PS69 in 2006 (Gohl, 2007) and PS104 in 2017 (Gohl, 2017). Twenty-five surface sediment samples from the southeastern and southwestern Weddell Sea continental shelf were collected during expeditions PS111 in 2018 (Schröder, 2018) and PS118 in 2019 (Dorschel, 2019). This new data set was complemented by data from 26 surface sediment samples collected in Bransfield Strait/WAP, which had been previously published by Vorrath et al. (2019).

3.2 Bulk sediment and organic geochemical analyses

The sediment material was freeze-dried and homogenized with an agate mortar and stored in glass vials at -20 °C before and after these initial preparation steps to avoid degradation of targeted molecular components. Total organic carbon (TOC) contents were measured on 0.1 g of sediment after removing inorganic carbon (total inorganic carbon, carbonates) with 500 µl 12 N hydrochloric acid. TOC contents were determined with a carbon-sulphur analyzer (CS 2000; Eltra) with standards for calibration being routinely measured before sample analysis and after every tenth sample (error ± 0.02 %).

Lipid biomarkers were extracted from the sediments (4 g for PS69 and PS104; 6 g for PS111 and PS118) by ultrasonication (3 x 15 min) using dichloromethane:methanol (3 x 6 ml for PS69 and PS104; 3 x 8 ml for PS111 and PS118; 2:1 v/v) as solvent. Prior to this step, the internal standards 7-hexylnonadecane (7-HND; 0.038 µg/sample for PS69 and PS104 and 0.057 µg/sample for PS111 and PS118), 5α-androstan-3-ol (1.04 µg/sample) and C_{46} (0.98 µg/sample) were added to the sample for quantification of HBIs, sterols and GDGTs, respectively. Via open-column chromatography, with SiO_2 as stationary phase, fractionation of the extract was achieved by eluting the apolar fraction (HBIs) and the polar fraction (sterols and GDGTs) with 5 ml n-hexane and 5 ml DCM/MeOH 1:1, respectively. The polar fraction was subsequently split into two fractions (sterols and GDGTs) for further processing. The sterol fraction was silylated with 300 µl bis-trimethylsilyl-trifluoroacetamide (BSTFA; 2h at 60 °C).

Compound analyses of HBIs and sterols were carried out on an Agilent Technologies 7890B gas chromatograph (GC; fitted with a 30 m DB 1MS column; 0.25 mm diameter and 0.25 µm film thickness) coupled to an Agilent Technologies 5977B mass selective detector (MSD; with 70 eV constant ionization potential, ion source temperature of 230 °C). The GC oven was set to: 60 °C (3 min), 150 °C (rate: 15 °C/min), 320 °C (rate: 10 °C/min), 320 °C (15 min isothermal) for the analysis of hydrocarbons and to: 60 °C (2 min), 150 °C (rate: 15 °C/min), 320 °C (rate: 3 °C/min), 320 °C (20 min isothermal) for the analysis of sterols. Helium was used as carrier gas. The HBI and sterol compounds were identified by their GC retention times and mass spectra (Belt, 2018; Belt et al., 2000; Boon et al., 1979). Lipids were quantified by setting the individual, manually integrated, GC-MS peak area in relation to the peak area of the respective internal standard and normalization to the amount of extracted sediment. $IPSO_{25}$ and HBI-trienes were quantified by relating their molecular ions ($IPSO_{25}$: m/z 348 and HBI-trienes: m/z 346) to the fragment ion m/z 266 of the internal standard 7-HND (Belt, 2018). Sterols were quantified by comparing the molecular ion of the individual sterol with the molecular ion m/z 348 of the internal standard 5α-androstan-3-ol. Instrumental response factors for the target lipids were considered as recommended by Belt et al. (2014) and Fahl and Stein (2012). All biomarker concentrations were subsequently normalized to the TOC content of each sample to account for different depositional settings within the different study areas.

For calculating the phytoplankton-$IPSO_{25}$ ($PIPSO_{25}$) index, we used the equation introduced by Vorrath et al. (2019):

$$PIPSO_{25} = IPSO_{25} / (IPSO_{25} + (\text{phytoplankton marker} \times c)) \qquad (1)$$

where c (c = mean $IPSO_{25}$/mean phytoplankton marker) is applied as a concentration balance factor to account for high concentration offsets between $IPSO_{25}$ and the phytoplankton biomarker (see Table S1 for c-factors of individual $PIPSO_{25}$ calculations).

Following the approach by Müller and Stein (2014) and Lamping et al. (2020), a $PIPSO_{25}$ value of 1 was assigned to samples with exceptionally low (at detection limit) concentrations of both biomarkers (see chapter 4.1.2). This comprises the five Weddell Sea samples PS111/13-2, /15-1, /16-3, /29-3 and /40-2 (marked as orange x in Fig. 1).

222 The GDGT fraction was dried under N_2, redissolved with 120 µl hexane:isopropanol (v/v 99:1) and

223 then filtered using a polytetrafluoroethylene (PTFE) filter with a 0.45 µm pore sized membrane. GDGTs

224 were measured using high performance liquid chromatography (HPLC; Agilent 1200 series HPLC

225 system) coupled to an Agilent 6120 mass spectrometer (MS), operating with atmospheric pressure

226 chemical ionization (APCI). The injection volume was 20 µl. For separating the GDGTs, a Prevail

227 Cyano 3 µm column (Grace, 150 mm * 2.1 mm) was kept at 30 °C. Each sample was eluted isocratically

228 for 5 min with solvent A = hexane/2-propanol/chloroform; 98:1:1 at a flow rate of 0.2 ml/min, then the

229 volume of solvent B = hexane/2-propanol/chloroform; 89:10:1 was increased linearly to 10 % within

230 20 min and then to 100 % within 10 min. The column was back-flushed (5 min, flow 0.6 ml/min) after

231 7 min after each sample and re-equilibrated with solvent A (10 min, flow 0.2 ml/min). The APCI was

232 set to the following: N_2 drying gas flow at 5 l/min and temperature to 350 °C, nebulizer pressure to 50

233 psi, vaporizer gas temperature to 350 °C, capillary voltage to 4 kV and corona current to +5 µA.

234 Detection of GDGTs was achieved by means of selective ion monitoring (SIM) of $[M+H]^+$ ions (dwell

235 time 76 ms). GDGT-0 (*m/z* 1302), GDGT-1 (*m/z* 1300), GDGT-2 (*m/z* 1298), GDGT-3 (*m/z* 1296) and

236 crenarchaeol (*m/z* 1292) as well as brGDGT-III (*m/z* 1050), brGDGT-II (*m/z* 1036) and brGDGT-I (*m/z*

237 1022) were quantified by relating their molecular ions to the molecular ion *m/z* 744 of the internal

238 standard C_{46}-GDGT. The late eluting hydroxylated GDGTs (OH-GDGT-0, OH-GDGT-1 and OH-

239 GDGT-2 with *m/z* 1318, 1316 and 1314, respectively) were quantified in the scans (*m/z* 1300, 1298,

240 1296) of their related GDGTs, as described by Fietz et al. (2013).

241 TEX^L_{86} values and their conversion into SOTs were determined following Kim et al. (2012):

242 $$TEX^L_{86} = LOG \frac{[GDGT-2]}{[GDGT-1]+[GDGT-2]+[GDGT-3]}, \tag{2}$$

243 $$SOT^{TEX} [°C] = 50.8 \times TEX^L_{86} + 36.1. \tag{3}$$

244 Temperature calculations based on OH-GDGTs were carried out according to Lü et al. (2015):

245 $$RI-OH' = \frac{[OH-GDGT-1]+2 \times [OH-GDGT-2]}{[OH-GDGT-0]+[OH-GDGT-1]+[OH-GDGT-2]}, \tag{4}$$

246 $$SST^{OH} [°C] = RI-OH' - 0.1/0.0382. \tag{5}$$

247 To determine the relative influence of terrestrial organic matter input, the Branched Isoprenoid

248 Tetraether (BIT)-index was calculated following Hopmans et al. (2004):

249 $$BIT = \frac{[brGDGT-I]+[brGDGT-II]+[brGDGT-III]}{[Chrenarchaeol]+[brGDGT-I]+[brGDGT-II]+[brGDGT-III]}. \tag{6}$$

250

3.3 Numerical model

3.3.1 Model description

253 AWI-ESM2 is a state-of-the-art coupled climate model developed by Sidorenko et al. (2019) which

254 comprises an atmospheric component ECHAM6 (Stevens et al., 2013) as well as an ocean-sea ice

255 component FESOM2 (Danilov et al., 2017). The atmospheric module ECHAM6 is the most recent

256 version of the ECHAM model developed at the Max Planck Institute for Meteorology (MPI) in

257 Hamburg. The model is branched from an early release of the European Center (EC) for Medium Range

258 Weather Forecasts (ECMWF) model (Roeckner et al., 1989). ECHAM6 dynamics is based on

259 hydrostatic primitive equations with traditional approximation. We used a T63 Gaussian grid with a

260 spatial resolution of about 1.9 x 1.9 degree (1.9 ° or 210 km). There are 47 vertical layers in the

261 atmosphere.

262 Momentum transport arising from boundary effects is configured using the subgrid orography scheme

263 as described by Lott (1999). Radiative transfer in ECHAM6 is represented by the method described in

264 Iacono et al. (2008). ECHAM6 also contains a Land-Surface Model (JSBACH) which includes 12

265 functional plant types of dynamic vegetation and 2 bare-surface types (Loveland et al., 2000; Raddatz

266 et al., 2007). The ice-ocean module in AWI-ESM2 is based on the finite volume discretization

267 formulated on unstructured meshes. The multi-resolution for the ocean is up to 15 km over polar and

268 coastal regions, and 135 km for far-field oceans, with 46 uneven vertical depths. The impact of local

269 dynamics on the global ocean is related to a number of FESOM-based studies (Danilov et al., 2017).

270 The multi-resolution approach advocated by FESOM allows to explore the impact of local processes

271 on the global ocean with moderate computational effort (Danilov et al., 2017). AWI-ESM2 employs

272 the OASIS3-MCT coupler (Valcke, 2013) with an intermediate regular exchange grid. Mapping

273 between the intermediate grid and the atmospheric/oceanic grid is handled with bilinear interpolation.

274 The atmosphere component computes 12 air–sea fluxes based on four surface fields provided by the

275 ocean module FESOM2. AWI-ESM2 has been validated under modern climate conditions (Sidorenko

276 et al., 2019) and has been applied for marine radiocarbon concentrations (Lohmann et al., 2020), the

277 latest Holocene (Vorrath et al., 2020), and the Last Interglacial (Otto-Bliesner et al., 2021).

278

279   3.3.2 Experimental design

280 One transient experiment was conducted using AWI-ESM2, which applied the boundary conditions,

281 including orbital parameters and greenhouse gases. Orbital parameters are calculated according to

282 Berger (1978), and the concentrations of greenhouse gases are taken from ice-core records and

283 measurements of recent firn air and atmospheric samples (Köhler et al., 2017). The model was

284 initialized from a 1,000-year spin-up run under mid-Holocene (6,000 before present, BP) boundary

285 conditions as described by Otto-Bliesner et al. (2017). In our modeling strategy, we follow Lorenz and

286 Lohmann (2004) and use the climate condition from the mid-Holocene spin-up run as the initial state

287 for the subsequent transient simulation covering the period from 6,000 BP to 2014 Common Era (CE).

288 In the present study we derived seasonal SIC, SSTs and SOTs in the study areas from a segment of the

289 transient experiment (1950-2014 CE). Topography including prescribed ice sheet configuration was

290 kept constant in our transient simulation. All model data are provided in Table S2.

291

292   3.4.   Satellite SIC and SSTs

293 Satellite sea-ice data were derived from Nimbus-7 SMMR and DMSP SSM/I-SSMIS passive

294 microwave data and downloaded from the National Snow and Ice Data Center (NSIDC; Cavalieri et al.,

295 1996). The sea-ice data represent mean monthly SIC, which are expressed to range from 0 % to 100 %

296 and are averaged over a period of the beginning of satellite observations in 1978 CE to the individual

297 year of sample collection. The monthly mean SIC were then split into different seasons: winter (JJF),

298 spring (SON) and summer (DJF) (Fig. 2a-c), and these data are considered to represent the recent mean

299 state of sea-ice coverage. All satellite data are provided in Table S3.

300 Modern annual mean SSTs and SOTs were derived from the World Ocean Atlas 2013 and represent

301 averaged values for the years 1955-2012 CE (WOA13; Locarnini et al., 2013).

302

303   **4.   Results and discussion**

304 In the following, we first present and discuss the biomarker data generated for this study from North

305 (Antarctic Peninsula) to South (Amundsen and Weddell seas) and draw conclusions about the

306 environmental settings deduced from the data set. In regard to the phytoplankton-derived biomarkers,

307 we focus on the significance of HBI Z-triene and brassicasterol, because the HBI E-triene and dinosterol

308 data, which are presented in the supplementary material (Fig. S1), show very similar patterns. All

309 biomarker data are provided in Table S1 and are available from the PANGAEA data repository

310 (https://doi.pangaea.de/10.1594/PANGAEA.932265). For the discussion of the target environmental

311 variables, *i.e.* PIPSO$_{25}$-based sea-ice and GDGT-derived ocean temperature estimates, satellite,

312 instrumental and model data are considered. In Sect. 5, we further address potential caveats in

313 biomarker-based environmental reconstructions that need to be taken into account when applying these

314 proxies.

315

316   4.1   TOC content, HBIs and sterols in Antarctic surface sediments

317 TOC contents in marine sediments are often viewed as an indicator for primary productivity in surface

318 waters (Meyers, 1997). However, we are aware that additional factors, such as different water depths

319 and depositional regimes, may exert control on sedimentary TOC as well. The TOC contents of the

320 investigated surface samples are lowest in Drake Passage with values around 0.12-0.54 % and increase

321 from northwest to southeast into Bransfield Strait, where they range from 0.59 to 1.06 % (Fig. 3a;

322 WAP). Along the EAP, higher TOC contents (0.57-0.86 %) prevail around the former Larsen A Ice

323 Shelf and north of James Ross Island but they decrease towards Powell Basin (0.22-0.37 %) and then

324 increase to 0.50 % around the South Orkney Islands, which may point to elevated productivity or

325 enhanced supply of reworked terrigenous organic matter in this area (Fig. 3a; EAP).
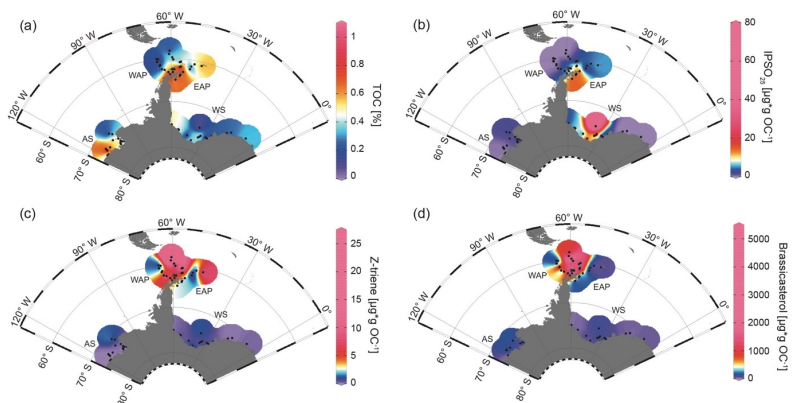
Fig. 3: Distribution of (a) TOC [%], (b) IPSO$_{25}$, (c) HBI Z-triene and (d) brassicasterol in surface sediment samples. Sample locations are marked as black dots. Concentrations of biomarkers [µg*g OC^{-1}] were normalized to the TOC content of each sample. AS: Amundsen Sea, WAP: West Antarctic Peninsula, EAP: East Antarctic Peninsula, WS: Weddell Sea.

326   At the WAP, concentrations of the sea-ice biomarker IPSO$_{25}$ increase from northwest to southeast.

327   IPSO$_{25}$ is absent in samples from the permanently ice-free Drake Passage and increases towards the

328   continental slope and the seasonally ice-covered shelf (0.37-17.81 µg*g OC^{-1}; Fig. 3b; Vorrath et al.,

329   2019). Highest IPSO$_{25}$ concentrations are observed in samples of the northern Bransfield Strait. Here,

330   the inflow of waters from the Weddell Sea transports sea ice into Bransfield Strait (Vorrath et al., 2019).

331   Elevated IPSO$_{25}$ concentrations are also observed at the seasonally sea-ice covered EAP, where

332   relatively high concentrations of the sea-ice biomarker prevail in samples located in the area of the

333   former Larsen A Ice Shelf and north of James Ross Island (12.59-17.74 µg*g OC^{-1}; Fig. 3b). Because

334   these locations are influenced by the northward drift of sea ice within the Weddell Gyre (Fig. 1), the

335   elevated IPSO$_{25}$ concentrations could also result from sea ice advected from the southern Weddell Sea.

336   We suggest that the decrease of IPSO$_{25}$ concentrations towards the Powell Basin and the South Orkney

337   Islands (0.59-5.36 µg*g OC^{-1}; Fig. 3b) is connected to warmer ocean temperatures in the North and

338   reduced sea-ice cover during spring.

339   Concentrations of the phytoplankton biomarker HBI Z-triene around the Antarctic Peninsula are highest

340   in eastern Drake Passage and along the WAP continental slope (where IPSO$_{25}$ is absent) and decrease

341   in Bransfield Strait (0.33-26.86 µg*g OC^{-1}; Fig. 3c; Vorrath et al., 2019). Elevated HBI Z-triene

342   concentrations have, so far, been detected in surface waters along the sea-ice edge (Smik et al., 2016)

343   and hence were suggested to be a proxy for marginal ice zone conditions (Belt et al., 2015; Collins et

344   al., 2013; Schmidt et al., 2018). Vorrath et al. (2019), however, relate the high concentrations of HBI

345   Z-triene at the northernmost stations in the permanently ice-free eastern Drake Passage to their

346   proximity to the Antarctic Polar Front. Here, productivity of the source diatoms of HBI-trienes (*e.g.*,

347   *Rhizosolenia* spp.; Belt et al., 2017) may be enhanced by meander-induced upwelling leading to

348   increased nutrient flux to surface waters (Moore and Abbott, 2002). Since Cárdenas et al. (2019)

349   document only minor abundances of *Rhizosolenia* spp. in seafloor surface sediments from this area, we

350   assume that HBI-trienes might also be biosynthesized by other diatom taxa. Moderate concentrations

351   along the continental slope of the WAP and in Bransfield Strait were associated with elevated inflow

352   of warm BSW which leads to a retreating sea-ice margin during spring and summer (for more details,

353   see Vorrath et al., 2019; 2020). Samples from the EAP shelf and Powell Basin are characterised by

354   relatively low HBI Z-triene concentrations (Fig. 3c; 0.1-2.37 µg*g OC^{-1}) that decrease from southwest

355   to northeast, whereas the northernmost sample closest to the South Orkney Islands is characterized by

356   an elevated HBI Z-triene concentration of ~8.49 µg*g OC^{-1} (Fig. 3c; EAP). This relatively high

357   concentration may be related to an "Island Mass Effect", coined by Doty and Oguri (1956), which refers

358   to increased primary production around oceanic islands in comparison to surrounding waters. Nolting

359   et al. (1991) found extraordinarily high dissolved iron levels (as high as 50-60 nM) on the South Orkney

360   shelf, while Nielsdóttir et al. (2012) observed enhanced iron and Chl *a* concentrations in the vicinity of

361   the South Orkney Islands. These authors explain the increased dissolved iron levels with input from

362   seasonally retreating sea ice, which is recorded by satellites (Fig. 2a-c) and probably leads to substantial

363   annual phytoplankton blooms, which may also cause the elevated TOC content in the corresponding

364   seafloor sediment sample (Fig. 3a). Alternatively, remobilization of shelf sediments or vertical mixing

365   of iron-rich deep waters, leading to high iron contents in surface waters, may stimulate primary

366   productivity (Blain et al., 2007; de Jong et al., 2012). However, it remains unclear why the brassicasterol

367   concentration is distinctly low in this sample, and we assume that different environmental preferences

368   of the source organisms may account for this. In Drake Passage and along the EAP, brassicasterol

369 displays a similar pattern as HBI Z-triene, with relatively high concentrations (more than 2 orders of

370 magnitudes) ranging from 1.86 to 5017.44 µg*g OC^{-1} (Fig. 3d).

371 In the Weddell Sea, TOC contents are generally low (< 0.4 %), with slightly elevated values in the West

372 (up to 0.50 %) and right in front of the Filchner Ice Shelf (up to 0.52 %; Fig. 3a). The Amundsen Sea

373 is characterized by slightly higher TOC contents, with concentrations of up to 0.91 % in the West and

374 lower values in the East (0.33 %; Fig. 3a; AS).

375 In the samples from the Amundsen and Weddell seas, that both are dominated by strong winter sea-ice

376 cover lasting until spring (Fig. 2a-c), all three biomarkers are present in low concentrations only. An

377 exception are the samples located in front of the Filchner Ice Shelf with significantly higher

378 concentrations of IPSO$_{25}$ (7.09-73.87 µg*g OC^{-1}; Fig. 3b; WS). Concentrations of IPSO$_{25}$ on the

379 Amundsen Sea shelf are relatively low (0.04-3.3 µg*g OC^{-1}), with slightly higher values observed in

380 the north-east (Fig. 3b; AS). HBI Z-triene concentrations are also very low, but slightly higher in

381 Filchner Trough (0.04-1 µg*g OC^{-1}) and at more distal locations on the northeastern Amundsen Sea

382 shelf (0.01-1.88 µg*g OC^{-1}; Fig. 3c). Brassicasterol generally shows a similar pattern as HBI Z-triene,

383 with concentrations varying between 1.86 and 220.54 µg*g OC^{-1} (Fig. 3d; for HBI E-triene and

384 dinosterol distribution, see Fig. S1).

385

386   4.2   Combining individual biomarker records: the PIPSO$_{25}$ index

387 The PIPSO$_{25}$ index combines the relative concentrations of IPSO$_{25}$ and a selected phytoplankton

388 biomarker, such as HBI-trienes and sterols, as indicator for an open-ocean environment (Vorrath et al.,

389 2019). The combination of both end members (sea ice vs. open-ocean) prevents misleading

390 interpretations regarding the absence of IPSO$_{25}$ in the sediments, which can be the result of two entirely

391 different scenarios. Under heavy/perennial sea-ice coverage, the thickness of sea ice hinders light

392 penetration, thereby limiting the productivity of algae living in basal sea ice (Hancke et al., 2018). This

393 scenario can cause the absence of both phytoplankton and sea-ice biomarkers in the sediment. The other

394 scenario depicts a permanently open ocean, where the sea-ice biomarker is absent as well, but here the

395 phytoplankton biomarkers are present in variable concentrations (Müller et al., 2011). The presence of

396 both biomarkers in the sediment is indicative of seasonal sea-ice coverage and/or the occurrence of

397 stable sea-ice margin conditions, promoting biosynthesis of both biomarkers (Müller et al., 2011). We

398 here distinguish between P$_Z$IPSO$_{25}$ and P$_B$IPSO$_{25}$ using HBI Z-triene and brassicasterol as

399 phytoplankton biomarker, respectively (Fig. 4a+b; for PIPSO$_{25}$ values based on HBI E-triene and

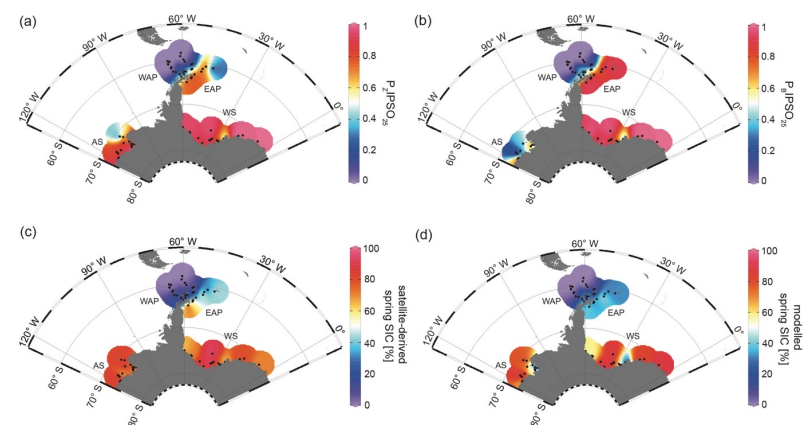400 dinosterol see Table S1 and Fig. S2).

Fig. 4: Distribution of the sea-ice index PIPSO$_{25}$ in surface sediment samples, with (a) P$_Z$IPSO$_{25}$ based on HBI Z-triene and (b) P$_B$IPSO$_{25}$ based on brassicasterol, (c) satellite-derived spring SIC [%] and (d) modelled spring SIC [%]. AS: Amundsen Sea, WAP: West Antarctic Peninsula, EAP: East Antarctic Peninsula, WS: Weddell Sea.

401 Both PIPSO$_{25}$ indices are 0 in the predominantly ice-free Drake Passage and increase towards southeast

402 to intermediate values on the WAP slope and around the South Shetland Islands, reflecting increased

403 influence of marginal sea-ice cover towards the coast (0.02-0.70; Vorrath et al., 2019). At the seasonally

404 sea-ice covered EAP, P$_Z$IPSO$_{25}$ values reach 0.84, while lower values of around 0.25 are observed close

405 to the South Orkney Islands, which is caused by the elevated HBI Z-triene concentrations at the stations

406 there (Fig. 3c; EAP). The P$_B$IPSO$_{25}$ index exhibits even higher values of up to 0.98 at the

407 EAP/northwestern Weddell Sea. These elevated PIPSO$_{25}$ indices align well with the significant

408 northward sea-ice drift within the Weddell Gyre, which leads to prolonged sea-ice cover along the EAP.

409 In samples from the southern Weddell Sea, both PIPSO$_{25}$ indices show a similar pattern with high values

410 up to 0.9, and slightly lower values in front of the Brunt Ice Shelf (0.6; Fig. 4a+b). Very low

411 concentrations (close to detection limit) of both biomarkers in samples from the continental shelf off

412 Dronning Maud Land (Fig. 1) result in low PIPSO$_{25}$ values, strongly underestimating the sea-ice cover

413 in this area, where satellite-derived sea-ice data document severe seasonal sea-ice cover (Fig. 2). As

414 previously mentioned, we followed the approach by Müller and Stein (2014) and Lamping et al. (2020)

415 by assigning a maximum PIPSO$_{25}$ value of 1 to these samples to circumvent misleading interpretations

416 and aid visualisation.

417 The intermediate PIPSO$_{25}$ value (~0.51) derived for one sample collected in front of the Brunt Ice Shelf

418 points to a less severe sea-ice cover in that area. A possible explanation for the relatively low PIPSO$_{25}$

419 value is the presence of a coastal polynya that has been reported by Anderson (1993) and which is

420 further supported by Paul et al. (2015). These authors note that the sea-ice area around the Brunt Ice

421 Shelf is the most active in the southern Weddell Sea, with an annual average polynya area of 3516 ±

422 1420 km². Interestingly, the reduced SIC here is also captured by our model (see Sect. 4.3).

423 PIPSO$_{25}$ values in the Amundsen Sea point to different scenarios. The P$_Z$IPSO$_{25}$ index varies around

424 0.9, with only the easterly, more distal samples having lower values between 0.3 and 0.6 (Fig. 4a). The

425 P$_B$IPSO$_{25}$ index generally has lower values, ranging from 0.6 in the coastal area to 0.2 in the more distal

426 samples (Fig. 4b). This difference between P$_Z$IPSO$_{25}$ and P$_B$IPSO$_{25}$ may be explained by the different

427 source organisms biosynthesizing the individual phytoplankton biomarkers. While the main

428 origin of HBI-trienes seems to be restricted to diatoms (Belt et al., 2017), brassicasterol is known to

429 be produced by several algal groups that are adapted to a wider range of sea surface conditions

430 (Volkman, 2006; see Sect. 5.2).

431

432   4.3   Biomarker-based sea ice estimates vs. satellite and model data

433 The main ice algae bloom in the Southern Ocean occurs during spring, when solar insolation and air

434 temperatures/SSTs increase and sea ice starts to melt, which results in the release of nutrients and

435 stratification of the water column stimulating the productivity of photosynthesizing organisms (Arrigo,

436 2017; Belt, 2018). The sea-ice biomarker IPSO$_{25}$ is hence commonly interpreted as a spring sea-ice

437 indicator, which is why, in the following, we compare the biomarker-based sea-ice reconstructions to

438 satellite-derived and modelled spring SIC. IPSO$_{25}$ concentrations in the surface sediments around the

439 Antarctic Peninsula exhibit similar trends as the satellite-derived and modelled SIC (Figs. 3+4), while

440 they differ significantly in the Amundsen and Weddell seas, where high SIC are recorded by satellites

441 and the model but IPSO$_{25}$ is present in low concentrations. The low IPSO$_{25}$ concentrations in these areas

442 highlight the uncertainty, when considering IPSO$_{25}$ as a sea-ice proxy alone, since such low

443 concentrations are not only observed under open water conditions, but also under severe sea-ice cover.

444 In the Amundsen and Weddell seas, the low IPSO$_{25}$ concentrations are the result of the latter, where

445 limited light availability hinders ice algae growth, leading to an underestimation of sea-ice cover.

446 Accordingly, we note a weak correlation between IPSO$_{25}$ data and satellite SIC (R² = 0.19; Fig. 5a). As

447 stated above, the combination of IPSO$_{25}$ and a phytoplankton marker may prevent this ambiguity. The

448 higher sea-ice concentrations in the Amundsen and Weddell seas are better reflected by maximum

449 P$_Z$IPSO$_{25}$ values than by IPSO$_{25}$ alone. However, we note that the P$_Z$IPSO$_{25}$ index apparently does not

450 resolve SICs higher than 50 % (see Fig. S3), which may indicate a threshold (here ~50 % SIC) where

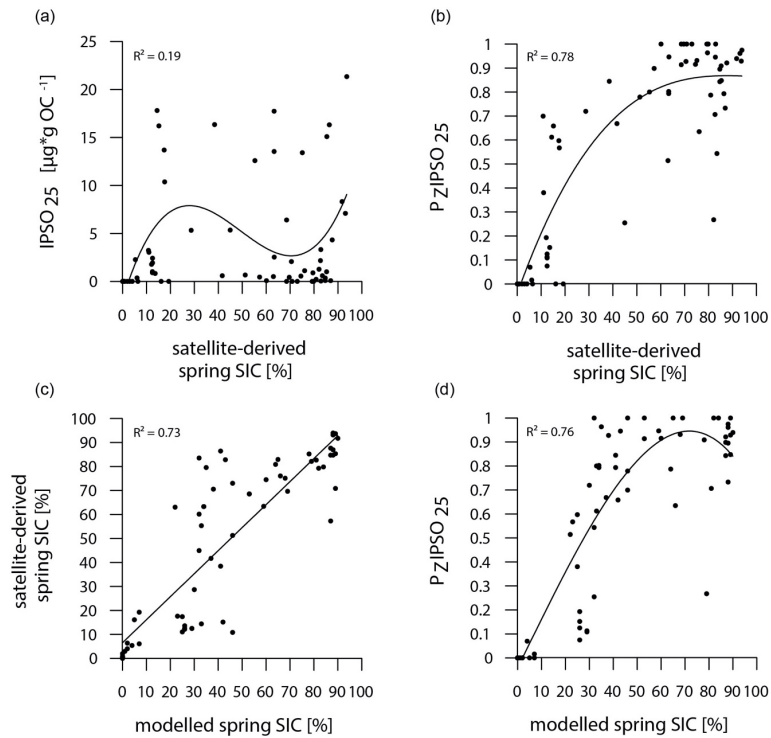451 the growth of the HBI-triene and IPSO$_{25}$ producing algae is limited.

(a)

$R^2 = 0.19$

IPSO$_{25}$ [μg*g OC^{-1}]

satellite-derived spring SIC [%]

(b)

$R^2 = 0.78$

P$_Z$IPSO$_{25}$

satellite-derived spring SIC [%]

(c)

$R^2 = 0.73$

satellite-derived spring SIC [%]

modelled spring SIC [%]

(d)

$R^2 = 0.76$

P$_Z$IPSO$_{25}$

modelled spring SIC [%]

Fig. 5: Correlations of (a) IPSO$_{25}$ concentrations vs. satellite-derived spring SIC, (b) P$_Z$IPSO$_{25}$ values vs. satellite-derived spring SIC, (c) satellite-derived spring SIC vs. modelled spring SIC and (d) P$_Z$IPSO$_{25}$ values vs. modelled spring SIC. Coefficients of determination (R^2) are given for the respective regression lines.

452   In general, however, the P$_Z$IPSO$_{25}$ values correlate much better with satellite and modelled SIC (R^2 =

453   0.78 and R^2 = 0.76, respectively; Fig. 5b+d) than IPSO$_{25}$ concentrations. Correlations of satellite and

454   model data with PIPSO$_{25}$ calculated using the HBI E-triene, brassicasterol and dinosterol, respectively,

455   are also positive but less significant (Fig. S4), and we hence focus the discussion on P$_Z$IPSO$_{25}$. The AWI-

456   ESM2-derived spring SICs correctly display the permanently ice-free Drake Passage and the northwest-

457   southeast increase in sea-ice cover from the WAP continental slope towards Bransfield Strait (Fig. 4d).

458   The model, however, significantly underestimates the elevated sea-ice concentrations (up to 70 %) in

459   front of the former Larsen Ice Shelf A and east of James Ross Island at the EAP observed in satellite

460   data. In the Amundsen and Weddell seas, the model predicts heavy sea-ice cover (~90 %), only slightly

461   underestimating the sea-ice cover at the near-coastal sites in front of Pine Island Glacier and Ronne Ice

462   Shelf. Interestingly, modelled SIC in front of Brunt Ice Shelf is as low as ~45 % (Fig. 4d+e),

463   corresponding well with the reduced P$_Z$IPSO$_{25}$ value of ~0.51. This may reflect the polynya conditions

464   in that region documented by Anderson (1993) and Paul et al. (2015). Overall, we note that modelled

465   modern SICs correlate well with satellite data (R^2 = 0.73; Fig. 5c) and P$_Z$IPSO$_{25}$ values (R^2 = 0.76; Fig.

466   5d), while we observe weaker correlations between modelled paleo-SICs and P$_Z$IPSO$_{25}$ values (Fig. S5;

467   see Sect. 5.1).

468

469   4.4   TEX$^L_{86}$- and RI-OH'-derived ocean temperatures

470   For a critical appraisal of the applicability and reliability of GDGT indices as temperature proxies in

471   polar latitudes, we here focus on the TEX$^L_{86}$ proxy by Kim et al. (2012), which potentially reflects

472   SOTs, and the RI-OH' proxy by Lü et al. (2015), which is assumed to reflect SSTs. The reconstructions

473   are believed to represent annual mean ocean temperatures (for correlations of TEX$^L_{86}$-derived SOTs

474   with WOA spring and winter SOTs, see Fig. S6). In all samples, the BIT-index (Eq. 6) is <0.3, indicating

475   no significant impact of terrestrial input of organic material on the distribution of GDGTs and hence

476   their reliability as temperature proxy. RI-OH'-derived temperatures and TEX$^L_{86}$-derived SOTs both

477   show a similar pattern, but different temperature ranges between -2.62 to +4.67 °C and -2.38 to

478   +8.75 °C, respectively (Fig. 6a+b). At the WAP, RI-OH'- as well as TEX$^L_{86}$-derived temperatures

479   increase northwestwards across the Antarctic continental slope and into the permanently ice-free Drake

480   Passage, which are influenced by the ACC and relatively warm CDW (Orsi et al., 1995; Rintoul et al.,

481   2001). Temperatures decrease towards Bransfield Strait and the EAP, which are influenced by seasonal

482   sea-ice cover and relatively cold water from the Weddell Sea that branches off the Weddell Gyre

483   (Collares et al., 2018; Thompson et al., 2009). At the EAP, a southwestward decrease is observed, with

484 relatively low temperatures at the former Larsen A Ice Shelf and higher temperatures recorded in Powell

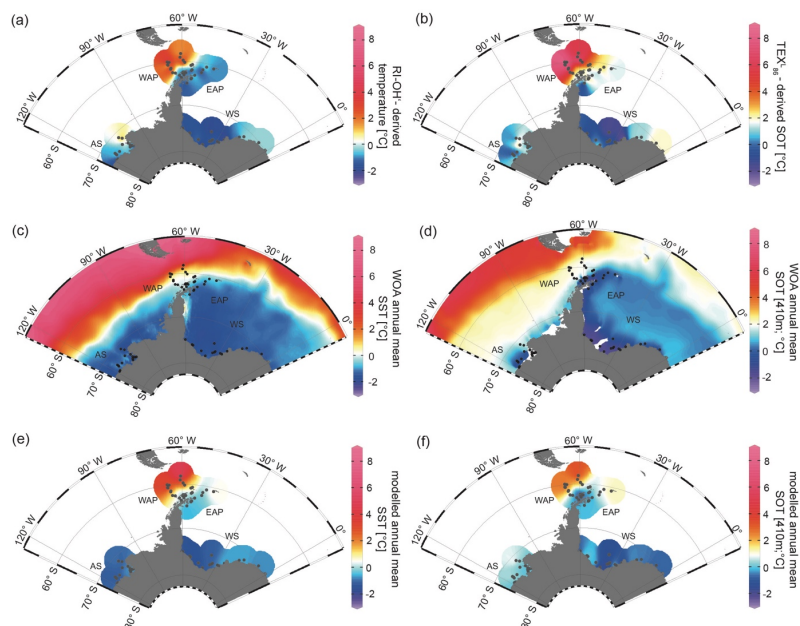485 Basin and around the South Orkney Islands (Fig. 6a+b).

Fig. 6: Annual mean temperature distributions with (a) RI-OH´-derived temperature, (b) TEX$^L_{86}$-derived SOT, (c) WOA13 SST (Locarnini et al., 2013), (d) WOA13 SOT (410 m; Locarnini et al., 2013), (e) modelled SST and (f) modelled SOT (410 m) in °C. AS: Amundsen Sea, WAP: West Antarctic Peninsula, EAP: East Antarctic Peninsula, WS: Weddell Sea.

486 In the Amundsen and Weddell seas further south, reconstructed temperatures are generally lower than

487 around the Antarctic Peninsula. Samples from the Weddell Sea display a temperature decrease from

488 east to west, which may reflect the route of eddies in the northeastern Weddell Gyre. These eddies

489 carry relatively warm, salty CDW westward along the southern limb of the Weddell Gyre, where it

490 becomes WDW (Vernet et al., 2019). Coldest TEX$^L_{86}$ and RI-OH' temperatures (<0 °C) at sites along

491 the Filchner-Ronne Ice Shelf front may be further linked to the presence of cold precursor water masses

492 for WSBW.

493 With regard to ongoing discussions, whether GDGT-based temperature reconstructions represent SSTs

494 or SOTs (Kalanetra et al., 2009; Kim et al., 2012; Park et al., 2019), we here compare our RI-OH' and

495 TEX$^L_{86}$-derived temperatures with surface and subsurface temperature data obtained by in-situ

496 measurements and modelling (Fig. 6c-f). Comparison of GDGT-derived temperatures with WOA13

497 temperatures from different water depths reveals the most significant correlation for a water depth of

498 410 m (for respective correlations, see Fig. S7). When discussing instrumental and modelled SOTs, we
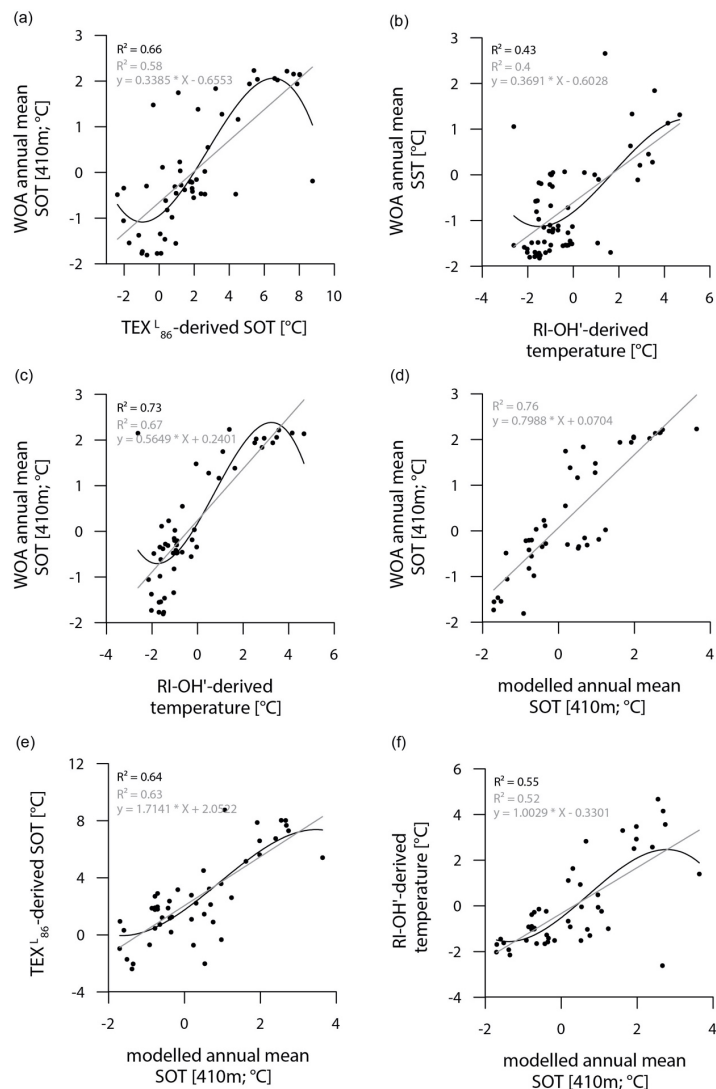
499 hence refer to 410 m water depth.

Fig. 7: Correlations of (a) WOA annual mean SOT (410 m) vs. TEX$^L_{86}$-derived SOT, (b) WOA annual mean SST vs. RI-OH'-derived temperature, (c) WOA annual mean SOT (410 m) vs. RI-OH'-derived temperature, (d) WOA annual mean SOT (410 m) vs. modelled annual mean SOT (410 m), (e) TEX$^L_{86}$-derived SOT vs. modelled annual mean SOT (410 m), (f) RI-OH'-derived temperature vs. modelled annual mean SOT (410 m) in °C. Coefficients of determination (R^2) are given for the respective regression lines.

500 While the correlation between TEX$^L_{86}$-derived SOTs and instrumental SOTs is reasonably good (Fig.

501 7a; R^2 = 0.66), also supporting a subsurface origin for the TEX$^L_{86}$ proxy, we note a significant

502 overestimation of SOTs by up to 6 °C in Drake Passage (Fig. S8). This warm-biased TEX$^L_{86}$ signal is a

503 known caveat and is, among others, assumed to be connected to GDGTs produced by deep-dwelling

504 Euryarchaeota (Park et al., 2019), which have been reported in CDW (Alonso-Sáez et al., 2011) and in

505 deep waters at the Antarctic Polar Front (López-García et al., 2001). Maximum TEX$^L_{86}$-based SOTs of

506 5 °C - 8 °C in central Drake Passage (Fig. 6b), however, distinctly exceed the common temperature

507 range of CDW (0-2 °C). Interestingly, TEX$^L_{86}$-derived SOTs in the colder regions of the Amundsen and

508 Weddell seas relate reasonably well to instrumental temperatures and are only slightly warm-biased

509 (Fig. S8). Correlations between RI-OH'-derived temperatures and instrumental SSTs are weak (R^2 =

510 0.43; Fig. 7b). Recently, Liu et al. (2020) concluded in their study on surface sediments from Prydz Bay

511 (East Antarctica), that also the RI-OH' index holds promise as a tool to reconstruct SOTs rather than

512 SSTs. When correlating our RI-OH'-derived temperatures with instrumental SOTs, we similarly find a

513 high correlation (R^2 = 0.73; Fig. 7c), hence supporting this hypothesis. We further note that the RI-OH'

514 temperature range is much more realistic than the TEX$^L_{86}$ range. This suggests that the addition of OH-

515 isoGDGTs in the temperature index is a promising step towards reliable high latitude temperature

516 reconstructions and may improve our understanding of the temperature responses of archaeal

517 membranes in Southern Ocean waters (Fietz et al., 2020; Park et al., 2019). Clearly, more data – ideally

518 obtained from sediment traps, seafloor surface sediment samples and longer sediment cores – and

519 calibration studies will help to further elucidate the applicability of the RI-OH' and TEX$^L_{86}$ temperature

520 reconstructions.

521 Similar to the model-derived sea-ice data, we also evaluate the model's performance in depicting ocean

522 temperatures (Fig. 6e+f). Modelled annual mean SSTs and SOTs are highest (with up to 5 °C and 3 °C,

523 respectively) in the permanently ice-free Drake Passage, which is influenced by the relatively warm

524 ACC. Lower SSTs are predicted for the Antarctic Peninsula continental slope and Bransfield Strait

525 (~0.5 to 1 °C), coinciding with the increase in the duration of seasonal sea-ice cover in that area. At the

526 EAP/northwestern Weddell Sea, modelled SSTs as well as SOTs increase from southwest to northeast

527 towards Powell Basin. In the Amundsen and Weddell seas, annual mean SSTs are negative, with

528 temperatures ranging from -1 to -0.5 °C, while SOTs are positive in the Amundsen Sea and negative in

529 the Weddell Sea. Overall, we note that modelled SOTs reflect instrumental SOTs reasonably well (R^2

530 = 0.76; Fig. 7d). Interestingly, while RI-OH'-derived SOTs relate better to instrumental SOTs (than

531 TEX^L_{86}-based SOTs), a better correlation between TEX^L_{86}-derived SOTs and modelled SOTs (R^2 =

532 0.64; Fig. 7e) and a weaker correlation with Ri-OH'-derived temperatures (R^2 = 0.55; Fig. 7f) is found.

533

534 **5. Caveats and recommendations for future research**

535 Marine core top studies evaluating the applicability and reliability of climate proxies are often affected

536 by limitations and uncertainties regarding the age control of the investigated seafloor surface sediments

537 as well as the production, preservation and degradation of target compounds. In the following, we

538 shortly address some of these factors and provide brief recommendations for future investigations.

539

540   5.1   Age control

541 Information on the actual age of the surface sediment samples is a major requirement determining their

542 suitability to reflect modern sea surface conditions. When comparing sea-ice conditions or ocean

543 temperatures estimated from biomarker data obtained from 0.5-1 cm thick surface sediment samples

544 (easily spanning decades to millennia, depending on sedimentation rates) with satellite-derived sea-ice

545 data or instrumental records (covering only the past ~40 and 65 years, respectively), the different time

546 periods reflected in the data sets need to be considered when interpreting the results. To address the

547 issue of lacking age constraints for most of the surface sediments investigated here, we also performed

548 paleoclimate simulations providing sea-ice concentration data for three time slices (2 ka, 4 ka and 6 ka

549 BP; see Fig. S5) to evaluate if the surface sediments may have recorded significantly older

550 environmental conditions. Correlations of PIPSO$_{25}$ values with these paleo sea-ice concentrations are

551 notably weaker (Fig. S5) than the correlations with recent (1951-2014 CE) SIC model output, which

552 points to a young to modern age of the majority of the studied sediments. This is further supported by

553 AMS ^{14}C-dating of calcareous microfossils and ^{210}Pb-dating of seafloor surface sediments from the

554 Amundsen Sea shelf documenting recent ages for most sites (Hillenbrand et al., 2010, 2013, 2017;

555 Smith et al., 2011, 2014, 2017; Witus et al., 2014) as well as modern ^{210}Pb-dates obtained for three

556 multicores collected in Bransfield Strait (PS97/56, PS97/68, PS97/72; Vorrath et al., 2020). AMS [14]C

557 dates obtained for nearby seafloor surface sediments in the vicinity of the South Shetland Islands and

558 the Antarctic Sound revealed ages of 100 years and 142 years BP, respectively (Vorrath et al., 2019).

559 As both uncorrected ages lie within the range of the modern marine reservoir effect (e.g. Gordon and

560 Harkness, 1992), we consider these two dates still as recent. However, in an area that is significantly

561 affected by rapid climate warming over the past decades and a regionally variable sea-ice coverage, the

562 age uncertainties for at least ^{14}C dated samples may easily lead to an over- or underestimation of

563 biomarker-based sea-ice cover and ocean temperatures, respectively, which needs to be taken into

564 account for comparisons with instrumental data. The utilization of (paleo-) model data may alleviate

565 the lack of age control for each seafloor sediment sample to some extent. Nevertheless, we recommend

566 that for a robust calibration of *e.g.*, PIPSO$_{25}$ values against satellite-derived sea-ice concentrations only

567 surface sediment samples with a modern age confirmed by ^{210}Pb-dating are incorporated.

568

569   5.2   Production and preservation of biomarkers

570 Biomarkers have the potential to reveal the former occurrence of their producers, which requires

571 knowledge of the source organisms. While there is general consensus on Thaumarchaeota being the

572 major source for iso-GDGTs (Fietz et al., 2020 and references therein) and diatoms synthesizing HBIs

573 (Volkman, 2006), the main source of brassicasterol, which is not only found in diatoms but also in

574 dinoflagellates and haptophytes (Volkman, 2006), remains unclear. Accordingly, the use of

575 brassicasterol to determine the PIPSO$_{25}$ index may introduce uncertainties regarding the environmental

576 information recorded by this phytoplankton biomarker. A further aspect concerns the different chemical

577 structures of HBIs and sterols, which raises the risk of a selective degradation (see Belt, 2018 and

578 Rontani et al., 2018; 2019 for detailed discussion) with potentially considerable effects on the PIPSO$_{25}$

579 index. Regarding the different areas investigated in our study, also spatially different microbial

580 communities and varying depositional regimes, such as sedimentation rate, redox conditions and water

581 depth, may lead to different degradation patterns. This means that variations in the biomarker

582   concentrations between different areas may not strictly reflect changes in the production of these

583   compounds (driven by sea surface conditions) but may also relate to different degradation states. In

584   particular, lower sedimentation rates and thus extended oxygen exposure times promote chemical

585   alteration and degradation processes (Hedges et al., 1990; Schouten et al., 2013). However, it has been

586   previously reported that the formation of mineral aggregates and fecal pellets often accelerates the

587   transport of organic matter from the sea surface through the water column to the seafloor during the

588   melting season, leading to a more rapid burial and hence better preservation of the organic compounds

589   (Bauerfeind et al., 2005; Etourneau et al., 2019; Müller et al., 2011).

590   Another rather technical drawback concerning the use of the PIPSO$_{25}$ index occurs when the

591   concentrations of the sea-ice proxy IPSO$_{25}$ and the phytoplankton marker are similarly low (due to

592   unfavourable conditions for both ice algae and phytoplankton) or similarly high (due to a significant

593   seasonal shift in sea-ice cover and/or stable ice edge conditions). This may lead to similar PIPSO$_{25}$

594   values, although the sea-ice conditions are fundamentally different from each other. This scenario is

595   evident for five sampling sites in the Weddell Sea (PS111/13-2, /15-1, /16-3, /29-3, and /40-2; Fig.

596   3b+c), where IPSO$_{25}$ and the HBI Z-triene concentrations are close to the detection limit and P$_Z$IPSO$_{25}$

597   values are very low, suggesting a reduced sea-ice cover. Satellite and model data, however, show that

598   these sample locations are influenced by heavy, nearly year-round sea-ice cover. We conclude that

599   biomarker concentrations of both biomarkers at or close to the detection limit need to be treated with

600   caution. Here, we assigned a maximum P$_Z$IPSO$_{25}$ value of 1 to those samples, and we note that such a

601   practice always needs to be clarified when applying the PIPSO$_{25}$ approach. Nonetheless, the coupling

602   of IPSO$_{25}$ with a phytoplankton marker provides more reliable sea-ice reconstructions. Regarding all

603   these ambiguities, we recommend not only to calculate the PIPSO$_{25}$ index, but also to carefully consider

604   individual biomarker concentrations and, if possible, to utilize other sea-ice proxies, such as data from

605   well-preserved diatom assemblages (Lamping et al., 2020; Vorrath et al., 2019; 2020). While the

606   PIPSO$_{25}$ index is not yet a fully quantitative proxy for paleo sea-ice concentrations, several calibration

607   iterations have been applied to the GDGT-paleothermometers (Fietz et al., 2020). As noted above, the

608   observation of distinctly warm-biased TEX$^{L}_{86}$-derived SOTs calls for further efforts of regional

609   calibration studies and/or investigations of archaean adaptation strategies at different water depths and

610   under different nutrient and temperature conditions.

611

612   5.3   The role of platelet ice for the production of IPSO$_{25}$

613   The sympagic, tube-dwelling, diatom *B. adeliensis* is a common constituent of Antarctic sea ice and

614   preferably flourishes in the relatively open channels of sub-ice platelet layers in near-shore locations

615   covered by fast ice (Medlin, 1990; Riaux-Gobin and Poulin, 2004). Based on investigations of sea-ice

616   samples from the Southern Ocean, Belt et al. (2016) detected this diatom species to be a source of

617   IPSO$_{25}$, which, according to its habitat, led to the assumption of the sea-ice proxy being a potential

618   indicator for the presence of platelet ice. As stated above, *B. adeliensis* is not confined to platelet ice,

619   but is also observed in basal sea ice and described as well adapted to changes in the texture of sea ice

620   during ice melt (Riaux-Gobin et al., 2013). Platelet ice formation, however, plays an important role in

621   sea-ice generation along some coastal regions of Antarctica (Hoppmann et al., 2015; 2020; Lange et al.,

622   1989; Langhorne et al., 2015). In these regions, CDW and High Saline Shelf Water (HSSW) flow into

623   sub-ice shelf cavities of ice shelves and cause basal melting and the discharge of cold and less saline

624   water (Fig. 8; Hoppmann et al., 2020, Scambos et al., 2017). The surrounding water is cooled and

625   freshened and is then transported towards the surface. Under the large Filchner-Ronne and Ross ice

626   shelves the pressure relief can cause this water, called Ice Shelf Water (ISW), to be supercooled (Foldvik

627   and Kvinge, 1974). The temperature of the supercooled ISW is typically below the in-situ freezing

628   point, which eventually causes the formation of ice platelets that accumulate under landfast ice attached

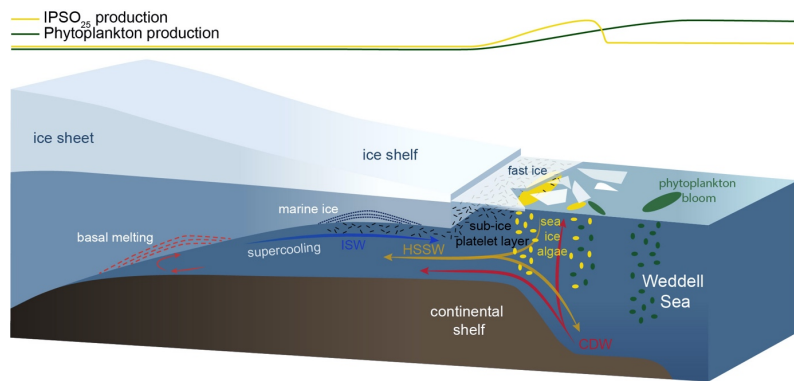629   to adjacent ice shelves (Fig. 8; Holland et al., 2007; Hoppmann et al., 2015; 2020).

Fig. 8: Schematic illustration of the formation of platelet ice and the main production areas of sea ice algae producing IPSO$_{25}$ (yellow ellipses) and phytoplankton (green ellipses), also displayed by yellow and green curves at the top. CDW: Circumpolar Deep Water, HSSW: High Saline Shelf Water, ISW: Ice Shelf Water. Illustration modified from Scambos et al. (2017).

630 In an attempt to elucidate the relationship between IPSO$_{25}$ and platelet ice, we investigated our data in

631 respect to locations of observed platelet ice formation. While the maximum IPSO$_{25}$ concentrations in

632 front of the Filchner Ice Shelf could be directly related to the above-mentioned platelet ice formation in

633 this area, the elevated IPSO$_{25}$ concentrations north of the Larsen C Ice Shelf at the EAP could be linked

634 to several processes. According to Langhorne et al. (2015), sea-ice cores retrieved from that area did

635 not incorporate platelet ice. The high IPSO$_{25}$ concentrations could hence be explained by either input

636 from drift ice transported with the Weddell Gyre or by basal freeze-on. However, we note that our

637 samples may reflect much longer time periods than the sea-ice samples investigated by Langhorne et

638 al. (2015) and the lack of platelet ice in their investigated sea-ice cores does not rule out the former

639 presence of platelet ice, which may be captured in our investigated sediment samples.

640 There are several previous studies on IPSO$_{25}$ that reported a close connection of the proxy with

641 proximal, coastal locations and polynyas in the seasonal ice zone (*i.e.* Collins et al., 2013; Smik et al.,

642 2016). They do not, however, discuss the relation to adjacent ice shelves as possible "platelet ice

643 factories". We note that the core locations investigated by Smik et al. (2016) are in the vicinity of the

644 Moscow University Ice Shelf, where Langhorne et al. (2015) did not observe platelet ice within sea-ice

645 cores. Hoppmann et al. (2020), however, report a sea-ice core from that area, which incorporates platelet

646 ice. The different observations by Langhorne et al. (2015) and Hoppmann et al. (2020) highlight the

647 temporal variability in the occurrence of platelet ice in the cold water regime around the East Antarctic

648 margin.

649 For the observed IPSO$_{25}$ minimum in the Amundsen Sea (Fig. 3b; AS), which we tentatively relate to

650 the extended and thick sea-ice coverage, the absence of platelet ice there is an alternative explanation.

651 The Amundsen/Bellingshausen seas and WAP shelves are classified as "warm shelves" (Thompson et

652 al., 2018), where the upwelling of warm CDW (Schmidtko et al., 2014) hinders the formation of ISW,

653 which makes the presence of platelet ice under recent conditions highly unlikely (Hoppmann et al.,

654 2020). This is also supported by Langhorne et al. (2015), who stated that platelet ice formation is not

655 observed in areas where basal ice-shelf melting is considerable, such as on the West Antarctic

656 continental shelf in the eastern Pacific sector of the Southern Ocean (Thompson et al., 2018).

657 Accordingly, if the formation and accumulation of platelet ice – up to a certain degree –indicates sub-

658 ice shelf melting on "cold shelves" (Hoppmann et al., 2015; Thompson et al., 2018), high IPSO$_{25}$

659 concentrations found in marine sediments may hence serve as indicator of past ISW formation and

660 associated ice shelf dynamics. This is, however, probably only true up to a certain threshold, where

661 platelet ice formation decreases or is hampered due to warm oceanic conditions causing too intense sub-

662 ice shelf melting (Langhorne et al., 2015).

663 When using IPSO$_{25}$ as a sea-ice proxy in Antarctica, it is important to consider regional platelet ice

664 formation processes, too, because these may affect the IPSO$_{25}$ budget. Determining thresholds

665 associated with platelet ice formation is challenging. Therefore, further investigations, such as in-situ

666 measurements of IPSO$_{25}$ concentrations in platelet ice or culture experiments in laboratories, are needed

667 to better understand the connection between IPSO$_{25}$ and platelet ice formation (and basal ice-shelf

668 melting).

669

670 **7. Conclusions**

671 Biomarker analyses focusing on IPSO$_{25}$, HBI-trienes, phytosterols and GDGTs in surface sediment

672 samples from the Antarctic continental margin were investigated to depict recent sea-ice conditions and

673 ocean temperatures in this climate sensitive region. Proxy-based reconstructions of these key variables

674 were compared to (1) satellite sea-ice data, (2) instrumental ocean temperature data, and (3) modelled

675 sea-ice patterns and ocean temperatures. The semi-quantitative sea-ice index PIPSO$_{25}$, combining the

676 sea-ice proxy IPSO$_{25}$ with an open-water phytoplankton marker, yielded reasonably good correlations

677 with satellite observations and numerical model results, while correlations with the sea-ice proxy IPSO$_{25}$

678 alone are rather low. Minimum concentrations of both biomarkers, used for the PIPSO$_{25}$ calculations,

679 may lead to ambiguous interpretations and significant underestimations of sea-ice conditions.

680 Therefore, different sea-ice measures should be considered when interpreting biomarker data.

681 Ocean temperature reconstructions based on the TEX$^L_{86}$- and RI-OH'-paleothermometers show similar

682 patterns, but different absolute temperatures. While TEX$^L_{86}$-derived temperatures are significantly

683 biased towards warm temperatures in Drake Passage, the RI-OH'-derived temperature range seems

684 more realistic when compared to temperature data based on the WOA13 and modelled annual mean

685 SOTs.

686 Further investigations of HBI- as well as GDGT-synthesis, transport, deposition and preservation within

687 the sediments would help to guide the proxies' application. Further work on the taxonomy of the IPSO$_{25}$

688 producers, the composition of their habitat (basal sea ice, platelet ice, brine channels) and its connection

689 to platelet ice formation via in-situ or laboratory measurements are required to better constrain the

690 IPSO$_{25}$ potential as a robust sea-ice biomarker. The presumed relationship between IPSO$_{25}$ and platelet

691 ice formation in connection to sub-ice shelf melting is supported by our data, showing high IPSO$_{25}$

692 concentrations in areas with known platelet ice formation and low IPSO$_{25}$ concentrations in areas

693 without observed platelet ice formation. Accordingly, oceanic conditions and the intensity of sub-ice

694 shelf melting need to be considered when using IPSO$_{25}$ (1) as an indirect indicator for sub-ice shelf

695 melting processes and associated ice shelf dynamics and (2) for the application of the PIPSO$_{25}$ index to

696 estimate sea-ice coverage.

697

698 **Data availability**

699 Datasets related to this article can be found online on *PANGAEA Data Publisher for Earth &*

700 *Environmental Science* (https://doi.pangaea.de/10.1594/PANGAEA.932265).

701

722 **References**

723 Abernathey, R. P., Cerovecki, I., Holland, P. R., Newsom, E., Mazloff, M., and Talley, L. D.: Water-

724 mass transformation by sea ice in the upper branch of the Southern Ocean overturning, Nature

725 Geoscience, 9, 596-601, 2016.

726 Allen, C. S., Pike, J., and Pudsey, C. J.: Last glacial–interglacial sea-ice cover in the SW Atlantic

727 and its potential role in global deglaciation, Quaternary Science Reviews, 30, 2446-2458, 2011.

728 Alonso-Sáez, L., Andersson, A., Heinrich, F., and Bertilsson, S.: High archaeal diversity in Antarctic

729   circumpolar deep waters, Environmental microbiology reports, 3, 689-697, 2011.

730 Anderson, P. S.: Evidence for an Antarctic winter coastal polynya, Antarctic science, 5, 221-226,

731   1993.

732 Armand, L. K., and Leventer, A.: Palaeo sea ice distribution–reconstruction and palaeoclimatic

733   significance, Sea ice—an introduction to its physics, biology, chemistry, and geology, 333-372,

734   2003.

735 Arrigo, K. R., Worthen, D. L., Lizotte, M. P., Dixon, P., and Dieckmann, G.: Primary production in

736   Antarctic sea ice, Science, 276, 394-397, 1997.

737 Arrigo, K. R.: Sea ice as a habitat for primary producers, Sea ice, 352-369, 2017.

738 Barbara, L., Crosta, X., Massé, G., and Ther, O.: Deglacial environments in eastern Prydz Bay, East

739   Antarctica, Quaternary Science Reviews, 29, 2731-2740, 2010.

740 Barbara, L., Crosta, X., Schmidt, S., and Massé, G.: Diatoms and biomarkers evidence for major

741   changes in sea ice conditions prior the instrumental period in Antarctic Peninsula, Quaternary

742   Science Reviews, 79, 99-110, 2013.

743 Bauerfeind, E., Leipe, T. and Ramseier, R.O.: Sedimentation at the permanently ice-covered

744   Greenland continental shelf (74°57.7'N/12°58.7'W): significance of biogenic and lithogenic

745   particles in particulate matter flux. Journal of Marine Systems 56, 151-166, 2005.

746 Belt, S. T., Allard, W. G., Massé, G., Robert, J.-M., and Rowland, S. J.: Highly branched isoprenoids

747   (HBIs): identification of the most common and abundant sedimentary isomers, Geochimica et

748   Cosmochimica Acta, 64, 3839-3851, 2000.

749 Belt, S. T., and Müller, J.: The Arctic sea ice biomarker IP_{25}: a review of current understanding,

750   recommendations for future research and applications in palaeo sea ice reconstructions,

751   Quaternary Science Reviews, 79, 9-25, 2013.

752 Belt, S. T., Brown, T. A., Ampel, L., Cabedo-Sanz, P., Fahl, K., Kocis, J. J., Masse, G., Navarro-

753   Rodriguez, A., Ruan, J., and Xu, Y.: An inter-laboratory investigation of the Arctic sea ice

754   biomarker proxy IP_{25} in marine sediments: key outcomes and recommendations, Climate of the

755   Past., 10, 155-166, 2014.

756 Belt, S. T., Cabedo-Sanz, P., Smik, L., Navarro-Rodriguez, A., Berben, S. M. P., Knies, J., and

757   Husum, K.: Identification of paleo Arctic winter sea ice limits and the marginal ice zone:

758   Optimised biomarker-based reconstructions of late Quaternary Arctic sea ice, Earth and Planetary

759   Science Letters, 431, 127-139, 2015.

760 Belt, S. T., Smik, L., Brown, T. A., Kim, J. H., Rowland, S. J., Allen, C. S., Gal, J. K., Shin, K. H.,

761   Lee, J. I., and Taylor, K. W. R.: Source identification and distribution reveals the potential of the

762   geochemical Antarctic sea ice proxy $IPSO_{25}$, Nature Communications, 7, 12655,

763   https://doi.org/10.1038/ncomms12655, 2016.

764 Belt, S. T., Brown, T. A., Smik, L., Tatarek, A., Wiktor, J., Stowasser, G., Assmy, P., Allen, C. S.,

765   and Husum, K.: Identification of C_{25} highly branched isoprenoid (HBI) alkenes in diatoms of the

766   genus Rhizosolenia in polar and sub-polar marine phytoplankton, Organic Geochemistry, 110,

767   65-72, 2017.

768 Belt, S. T.: Source-specific biomarkers as proxies for Arctic and Antarctic sea ice, Organic

769   Geochemistry, 125, 277-298, 2018.

770 Berger, A.: Long-term variations of daily insolation and Quaternary climatic changes, Journal of the

771   atmospheric sciences, 35, 2362-2367, 1978.

772 Blain, S., Quéguiner, B., Armand, L., Belviso, S., Bombled, B., Bopp, L., Bowie, A., Brunet, C.,

773   Brussaard, C., Carlotti, F., Christaki, U., Corbière, A., Durand, I., Ebersbach, F., Fuda, J.-L.,

774   Garcia, N., Gerringa, L., Griffiths, B., Guigue, C., Guillerm, C., Jacquet, S., Jeandel, C., Laan,

775   P., Lefèvre, D., Lo Monaco, C., Malits, A., Mosseri, J., Obernosterer, I., Park, Y.-H., Picheral,

776   M., Pondaven, P., Remenyi, T., Sandroni, V., Sarthou, G., Savoye, N., Scouarnec, L., Souhaut,

777   M., Thuiller, D., Timmermans, K., Trull, T., Uitz, J., van Beek, P., Veldhuis, M., Vincent, D.,

778   Viollier, E., Vong, L. and Wagener, T.: Effect of natural iron fertilization on carbon sequestration

779   in the Southern Ocean. Nature 446, 1070-1074, 2007.

780 Boon, J. J., Rijpstra, W. I. C., de Lange, F., De Leeuw, J., Yoshioka, M., and Shimizu, Y.: Black

781   Sea sterol—a molecular fossil for dinoflagellate blooms, Nature, 277, 125-127, 1979.

782 Cárdenas, P., Lange, C. B., Vernet, M., Esper, O., Srain, B., Vorrath, M.-E., Ehrhardt, S., Müller, J.,

783   Kuhn, G., and Arz, H. W.: Biogeochemical proxies and diatoms in surface sediments across the

Drake Passage reflect oceanic domains and frontal systems in the region, Progress in Oceanography, 174, 72-88, 2019.

Cavalieri, D., Parkinson, C., Gloersen, P., and Zwally, H.: Sea ice concentrations from Nimbus-7 SMMR and DMSP SSM/I passive microwave data, National Snow and Ice Data Center, Boulder, Colorado, USA, 1996.

Collares, L. L., Mata, M. M., Kerr, R., Arigony-Neto, J., and Barbat, M. M.: Iceberg drift and ocean circulation in the northwestern Weddell Sea, Antarctica, Deep Sea Research Part II: Topical Studies in Oceanography, 149, 10-24, 2018.

Colleoni, F., De Santis, L., Siddoway, C. S., Bergamasco, A., Golledge, N. R., Lohmann, G., Passchier, S., and Siegert, M. J.: Spatio-temporal variability of processes across Antarctic ice-bed–ocean interfaces, Nature Communications, 9, 2289, https://doi.org/10.1038/s41467-018-04583-0, 2018.

Collins, L. G., Allen, C. S., Pike, J., Hodgson, D. A., Weckström, K., and Massé, G.: Evaluating highly branched isoprenoid (HBI) biomarkers as a novel Antarctic sea-ice proxy in deep ocean glacial age sediments, Quaternary Science Reviews, 79, 87-98, 2013.

Comiso, J. C., Gersten, R. A., Stock, L. V., Turner, J., Perez, G. J., and Cho, K.: Positive Trend in the Antarctic Sea Ice Cover and Associated Changes in Surface Temperature, Journal of Climate, 30, 2251-2267, 2017.

Cook, A.J., Holland, P., Meredith, M., Murray, T., Luckman, A., Vaughan, D.G.: Ocean forcing of glacier retreat in the WAP. Science, 353, 283-286, 2016.

Crosta, X., Pichon, J. J., and Burckle, L.: Application of modern analog technique to marine Antarctic diatoms: Reconstruction of maximum sea-ice extent at the Last Glacial Maximum, Paleoceanography and Paleoclimatology, 13, 284-297, 1998.

Crosta, X., Etourneau, J., Orme, L.C., Dalaiden, Q., Campagne, P., Swingedouw, D., Goosse, H., Massé, G., Miettinen, A., McKay, R.M., Dunbar, R.B., Escutia, C. and Ikehara, M.: Multi-decadal trends in Antarctic sea-ice extent driven by ENSO–SAM over the last 2,000 years. Nature Geoscience 14, 156-160, 2021.

Danilov, S., Sidorenko, D., Wang, Q., and Jung, T.: The Finite-volumE Sea ice–Ocean Model (FESOM2), Geosci. Model Dev., 10, 765-789, 2017.de Jong, J., Schoemann, V., Lannuzel, D., Croot, P., de Baar, H. and Tison, J.-L.: Natural iron fertilization of the Atlantic sector of the Southern Ocean by continental shelf sources of the Antarctic Peninsula. Journal of Geophysical Research: Biogeosciences 117, 2012.

De Jong, J., Schoemann, V., Lannuzel, D., Croot, P., de Baar, H., and Tison, J. L.: Natural iron fertilization of the Atlantic sector of the Southern Ocean by continental shelf sources of the Antarctic Peninsula, Journal of Geophysical Research: Biogeosciences, 117, 2012.

Denis, D., Crosta, X., Barbara, L., Massé, G., Renssen, H., Ther, O., and Giraudeau, J.: Sea ice and wind variability during the Holocene in East Antarctica: insight on middle–high latitude coupling, Quaternary Science Reviews, 29, 3709-3719, 2010.

Dorschel, B.: The Expedition PS118 of the Research Vessel POLARSTERN to the Weddell Sea in 2019, Berichte zur Polar-und Meeresforschung = Reports on polar and marine research, 735, 2019.

Doty, M. S., and Oguri, M.: The island mass effect, ICES Journal of Marine Science, 22, 33-37, 1956.

Eayrs, C., Li, X., Raphael, M.N. and Holland, D.M.: Rapid decline in Antarctic sea ice in recent years hints at future change. Nature Geoscience 14, 460-464, 2021.

Esper, O., and Gersonde, R.: New tools for the reconstruction of Pleistocene Antarctic sea ice, Palaeogeography, Palaeoclimatology, Palaeoecology, 399, 260-283, 2014.

Etourneau, J., Collins, L. G., Willmott, V., Kim, J.-H., Barbara, L., Leventer, A., Schouten, S., Damsté, J. S., Bianchini, A., and Klein, V.: Holocene climate variations in the WAP: evidence for sea ice extent predominantly controlled by changes in insolation and ENSO variability, Climate of the Past, 9, 1431-1446, 2013.

Etourneau, J., Sgubin, G., Crosta, X., Swingedouw, D., Willmott, V., Barbara, L., Houssais, M.-N., Schouten, S., Damsté, J.S.S., Goosse, H.: Ocean temperature impact on ice shelf extent in the eastern Antarctic Peninsula. Nature Communications 10, 1-8, 2019.

838 Fahl, K., and Stein, R.: Modern seasonal variability and deglacial/Holocene change of central Arctic

839   Ocean sea-ice cover: new insights from biomarker proxy records, Earth and Planetary Science

840   Letters, 351, 123-133, 2012.

841 Fetterer, F., Knowles, K., Meier, W., Savoie, M., Windnagel, A.K., 2016. Updated Daily. Sea Ice

842   Index, Version 2. [Median Sea Ice Extent 1981-2010]. NSIDC: National Snow and Ice Data

843   Center, Boulder, Colorado USA. https://doi.org/10.7265/N5736NV7 [24 July 2017].

844 Fietz, S., Huguet, C., Rueda, G., Hambach, B., and Rosell-Melé, A.: Hydroxylated isoprenoidal

845   GDGTs in the Nordic Seas, Marine Chemistry, 152, 1-10, 2013.

846 Fietz, S., Ho, S., and Huguet, C.: Archaeal Membrane Lipid-Based Paleothermometry for

847   Applications in Polar Oceans, Oceanography, 33, 104-114, 2020.

848 Foldvik, A., and Kvinge, T.: Conditional instability of sea water at the freezing point, Deep Sea

849   Research and Oceanographic Abstracts, 21, 169-174, 1974.

850 Fretwell, P., Pritchard, H.D., Vaughan, D.G., 57 others. Bedmap2: improved ice bed, surface and

851   thickness datasets for Antarctica. Cryosphere 7, 375-393. http://dx.doi.org/10.5194/tc-7-375-

852   2013, 2013.

853 Gersonde, R., and Zielinski, U.: The reconstruction of late Quaternary Antarctic sea-ice

854   distribution—the use of diatoms as a proxy for sea-ice, Palaeogeography, Palaeoclimatology,

855   Palaeoecology, 162, 263-286, 2000.

856 Gohl, K.: The expedition ANTARKTIS-XXIII/4 of the research vessel Polarstern in 2006, Berichte

857   zur Polar-und Meeresforschung (Reports on Polar and Marine Research), 557, 2007.

858 Gohl, K.: The Expedition PS104 of the Research Vessel POLARSTERN to the Amundsen Sea in

859   2017, Berichte zur Polar-und Meeresforschung = Reports on polar and marine research, 712,

860   2017.

861 Gordon, J.E., Harkness, D.D.: Magnitude and geographic variation of the radiocarbon content in

862   Antarctic marine life: implications for reservoir corrections in radiocarbon dating, Quaternary

863   Science Reviews 11, 697-708, 1992.

864 Hancke, K., Lund-Hansen, L. C., Lamare, M. L., Højlund Pedersen, S., King, M. D., Andersen, P.,

865   and Sorrell, B. K.: Extreme low light requirement for algae growth underneath sea ice: A case

866   study from Station Nord, NE Greenland, Journal of Geophysical Research: Oceans, 123, 985-

867   1000, 2018.

868 Harms, S., Fahrbach, E., and Strass, V. H.: Sea ice transports in the Weddell Sea, Journal of

869   Geophysical Research: Oceans, 106, 9057-9073, 2001.

870 Hedges, J.I., Hu, F.S., Devol, A.H., Hartnett, H.E., Tsamakis, E. and Keil, R.G.: Sedimentary organic

871   matter preservation; a test for selective degradation under oxic conditions. Am J Sci 299, 529-

872   555, 1999.

873 Hellmer, H.H., Rhein, M., Heinemann, G., Abalichin, J., Abouchami, W., Baars, O., Cubasch, U.,

874   Dethloff, K., Ebner, L., Fahrbach, E., Frank, M., Gollan, G., Greatbatch, R.J., Grieger, J.,

875   Gryanik, V.M., Gryschka, M., Hauck, J., Hoppema, M., Huhn, O., Kanzow, T., Koch, B.P.,

876   König-Langlo, G., Langematz, U., Leckebusch, G.C., Lüpkes, C., Paul, S., Rinke, A., Rost, B.,

877   van der Loeff, M.R., Schröder, M., Seckmeyer, G., Stichel, T., Strass, V., Timmermann, R.,

878   Trimborn, S., Ulbrich, U., Venchiarutti, C., Wacker, U., Willmes, S. and Wolf-Gladrow, D.:

879   Meteorology and oceanography of the Atlantic sector of the Southern Ocean - a review of German

880   achievements from the last decade. Ocean Dynamics 66, 1379-1413, 2016.

881 Hillenbrand, C.-D., Smith, J.A., Kuhn, G., Esper, O., Gersonde, R., Larter, R.D., Maher, B.,

882   Moreton, S.G., Shimmield, T.M., Korte, M.: Age assignment of a diatomaceous ooze deposited

883   in the western Amundsen Sea Embayment after the Last Glacial Maximum. Journal of

884   Quaternary Science 25, 280-295, 2010.

885 Hillenbrand, C.-D., Kuhn, G., Smith, J.A., Gohl, K., Graham, A.G.C., Larter, R.D., Klages, J.P.,

886   Downey, R., Moreton, S.G., Forwick, M., Vaughan, D.G.: Grounding-line retreat of the West

887   Antarctic Ice Sheet from inner Pine Island Bay. Geology 41, 35-38, 2013.

888 Hillenbrand, C.-D., Smith, J.A., Hodell, D.A., Greaves, M., Poole, C.R., Kender, S., Williams, M.,

889   Andersen, T.J., Jernas, P.E., Elderfield, H., Klages, J.P., Roberts, S.J., Gohl, K., Larter, R.D.,

890   Kuhn, G.: West Antarctic Ice Sheet retreat driven by Holocene warm water intrusions. Nature

891   547, 43–48, 2017.

892 Ho, S. L., Mollenhauer, G., Fietz, S., Martínez-Garcia, A., Lamy, F., Rueda, G., Schipper, K.,

893   Méheust, M., Rosell-Melé, A., Stein, R., and Tiedemann, R.: Appraisal of TEX_{86} and

thermometries in subpolar and polar regions, Geochimica et Cosmochimica Acta, 131, 213-226, 2014.

Hobbs, W. R., Massom, R., Stammerjohn, S., Reid, P., Williams, G., and Meier, W.: A review of recent changes in Southern Ocean sea ice, their drivers and forcings, Global and Planetary Change, 143, 228-250, 2016.

Holland, P. R., Feltham, D. L., and Jenkins, A.: Ice shelf water plume flow beneath Filchner-Ronne Ice Shelf, Antarctica, Journal of Geophysical Research: Oceans, 112, https://doi.org/10.1029/2006JC003915, 2007.

Hopmans, E. C., Weijers, J. W., Schefuß, E., Herfort, L., Damsté, J. S. S., and Schouten, S.: A novel proxy for terrestrial organic matter in sediments based on branched and isoprenoid tetraether lipids, Earth and Planetary Science Letters, 224, 107-116, 2004.

Hoppmann, M., Nicolaus, M., Paul, S., Hunkeler, P. A., Heinemann, G., Willmes, S., Timmermann, R., Boebel, O., Schmidt, T., and Kühnel, M.: Ice platelets below Weddell Sea landfast sea ice, Annals of Glaciology, 56, 175-190, 2015.

Hoppmann, M., Richter, M. E., Smith, I. J., Jendersie, S., Langhorne, P. J., Thomas, D. N., and Dieckmann, G. S.: Platelet ice, the Southern Ocean's hidden ice: a review, Annals of Glaciology, 1-28, 2020.

Huguet, C., de Lange, G. J., Gustafsson, Ö., Middelburg, J. J., Damsté, J. S. S., and Schouten, S.: Selective preservation of soil organic matter in oxidized marine sediments (Madeira Abyssal Plain), Geochimica et Cosmochimica Acta, 72, 6061-6068, 2008.

Iacono, M. J., Delamere, J. S., Mlawer, E. J., Shephard, M. W., Clough, S. A., and Collins, W. D.: Radiative forcing by long-lived greenhouse gases: Calculations with the AER radiative transfer models, Journal of Geophysical Research: Atmospheres, 113, https://doi.org/10.1029/2008JD009944, 2008.

Jacobs, S. S., Jenkins, A., Giulivi, C. F., and Dutrieux, P.: Stronger ocean circulation and increased melting under Pine Island Glacier ice shelf, Nature Geoscience, 4, 519-523, 2011.

Jenkins, A., and Jacobs, S.: Circulation and melting beneath George VI ice shelf, Antarctica, Journal of Geophysical Research: Oceans, 113, https://doi.org/10.1029/2007JC004449, 2008.

Johns, L., Wraige, E., Belt, S., Lewis, C., Massé, G., Robert, J.-M., and Rowland, S.: Identification of a C_{25} highly branched isoprenoid (HBI) diene in Antarctic sediments, Antarctic sea-ice diatoms and cultured diatoms, Organic Geochemistry, 30, 1471-1475, 1999.

Kalanetra, K. M., Bano, N., and Hollibaugh, J. T.: Ammonia-oxidizing Archaea in the Arctic Ocean and Antarctic coastal waters, Environmental Microbiology, 11, 2434-2445, 2009.

Khazendar, A., Rignot, E., Schroeder, D.M., Seroussi, H., Schodlok, M.P., Scheuchl, B., Mouginot, J., Sutterley, T.C., Velicogna, I.: Rapid submarine ice melting in the grounding zones of ice shelves in West Antarctica. Nature communications 7, 1-8, 2016.

Kim, J.-H., Van der Meer, J., Schouten, S., Helmke, P., Willmott, V., Sangiorgi, F., Koç, N., Hopmans, E. C., and Damsté, J. S. S.: New indices and calibrations derived from the distribution of crenarchaeal isoprenoid tetraether lipids: Implications for past sea surface temperature reconstructions, Geochimica et Cosmochimica Acta, 74, 4639-4654, 2010.

Kim, J.-H., Crosta, X., Willmott, V., Renssen, H., Bonnin, J., Helmke, P., Schouten, S., and Sinninghe Damsté, J. S.: Holocene subsurface temperature variability in the eastern Antarctic continental margin, Geophysical Research Letters, 39, https://doi.org/10.1029/2012GL051157, 2012.

Klinck, J. M., Hofmann, E. E., Beardsley, R. C., Salihoglu, B., and Howard, S.: Water-mass properties and circulation on the WAP Continental Shelf in Austral Fall and Winter 2001, Deep Sea Research Part II: Topical Studies in Oceanography, 51, 1925-1946, 2004.

Köhler, P., Nehrbass-Ahles, C., Schmitt, J., Stocker, T. F., and Fischer, H.: A 156 kyr smoothed history of the atmospheric greenhouse gases CO_2, CH_4, and N_2O and their radiative forcing, Earth Syst. Sci. Data, 9, 363-387, 2017.

Lamping, N., Müller, J., Esper, O., Hillenbrand, C.-D., Smith, J. A., and Kuhn, G.: Highly branched isoprenoids reveal onset of deglaciation followed by dynamic sea-ice conditions in the western Amundsen Sea, Antarctica, Quaternary Science Reviews, 228, https://doi.org/10.1016/j.quascirev.2019.106103, 2020.

Lange, M., Ackley, S., Wadhams, P., Dieckmann, G., and Eicken, H.: Development of sea ice in the Weddell Sea, Annals of Glaciology, 12, 92-96, 1989.

950 Langhorne, P., Hughes, K., Gough, A., Smith, I., Williams, M., Robinson, N., Stevens, C., Rack,
951   W., Price, D., and Leonard, G.: Observed platelet ice distributions in Antarctic sea ice: An index
952   for ocean-ice shelf heat flux, Geophysical Research Letters, 42, 5442-5451, 2015.

953 Leventer, A.: The fate of Antarctic "sea ice diatoms" and their use as paleoenvironmental indicators,
954   Antarctic sea ice. Biological processes, interactions and variability, 121-137, 1998.

955 Li, X., Holland, D.M., Gerber, E.P. and Yoo, C.:Impacts of the north and tropical Atlantic Ocean on
956   the Antarctic Peninsula and sea ice. Nature 505, 538-542, 2014.

957 Liu, J., Curry, J. A., and Martinson, D. G.: Interpretation of recent Antarctic sea ice variability,
958   Geophysical Research Letters, 31, https://doi.org/10.1029/2003GL018732, 2004.

959 Liu, R., Han, Z., Zhao, J., Zhang, H., Li, D., Ren, J., Pan, J., Zhang, H.: Distribution and source of
960   glycerol dialkyl glycerol tetraethers (GDGTs) and the applicability of GDGT-based temperature
961   proxies in surface sediments of Prydz Bay, East Antarctica. Polar Research, 2020.

962 Locarnini, R. A., Mishonov, A. V., Antonov, J. I., Boyer, T. P., Garcia, H. E., Baranova, O. K.,
963   Zweng, M. M., Paver, C. R., Reagan, J. R., and Johnson, D. R.: World ocean atlas 2013. Volume
964   1, Temperature, NOAA Atlas NESDIS 73, 40 pp., doi: 10.7289/V55X26VD, 2013.

965 Lohmann, G., Butzin, M., Eissner, N., Shi, X., and Stepanek, C.: Abrupt climate and weather
966   changes across time scales, Paleoceanography and Paleoclimatology, 35,
967   https://doi.org/10.1029/2019PA003782, 2020.

968 López-García, P., Rodriguez-Valera, F., Pedrós-Alió, C., and Moreira, D.: Unexpected diversity of
969   small eukaryotes in deep-sea Antarctic plankton, Nature, 409, 603-607, 2001.

970 Lorenz, S. J., and Lohmann, G.: Acceleration technique for Milankovitch type forcing in a coupled
971   atmosphere-ocean circulation model: method and application for the Holocene, Climate
972   Dynamics, 23, 727-743, 2004.

973 Lott, F.: Alleviation of stationary biases in a GCM through a mountain drag parameterization scheme
974   and a simple representation of mountain lift forces, Monthly weather review, 127, 788-801, 1999.

975 Loveland, T. R., Reed, B. C., Brown, J. F., Ohlen, D. O., Zhu, Z., Yang, L., and Merchant, J. W.:
976   Development of a global land cover characteristics database and IGBP DISCover from 1 km
977   AVHRR data, Int. J. Remote Sens., 21, 1303-1330, 2000.

978 Lü, X., Liu, X.-L., Elling, F. J., Yang, H., Xie, S., Song, J., Li, X., Yuan, H., Li, N., and Hinrichs,
979   K.-U.: Hydroxylated isoprenoid GDGTs in Chinese coastal seas and their potential as a
980   paleotemperature proxy for mid-to-low latitude marginal seas, Organic Geochemistry, 89-90, 31-
981   43, 2015.

982 Massé, G., Belt, S. T., Crosta, X., Schmidt, S., Snape, I., Thomas, D. N., and Rowland, S. J.: Highly
983   branched isoprenoids as proxies for variable sea ice conditions in the Southern Ocean, Antarctic
984   Science, 23, 487-498, 2011.

985 Massom, R. A., Scambos, T. A., Bennetts, L. G., Reid, P., Squire, V. A., and Stammerjohn, S. E.:
986   Antarctic ice shelf disintegration triggered by sea ice loss and ocean swell, Nature, 558, 383-389,
987   2018.

988 Medlin, L.: Berkeleya spp. from Antarctic waters, including Berkeleya adeliensis, sp. nov., a new
989   tube dwelling diatom from the undersurface of sea-ice, Beihefte zur Nova Hedwigia, 100, 77-89,
990   1990.

991 Meredith, M. P., Woodworth, P. L., Chereskin, T. K., Marshall, D. P., Allison, L. C., Bigg, G. R.,
992   Donohue, K., Heywood, K. J., Hughes, C. W., and Hibbert, A.: Sustained monitoring of the
993   Southern Ocean at Drake Passage: Past achievements and future priorities, Reviews of
994   Geophysics, 49, https://doi.org/10.1029/2010RG000348, 2011.

995 Meyers, P. A.: Organic geochemical proxies of paleoceanographic, paleolimnologic, and
996   paleoclimatic processes, Organic geochemistry, 27, 213-250, 1997.

997 Moore, J. K., and Abbott, M. R.: Surface chlorophyll concentrations in relation to the Antarctic Polar
998   Front: seasonal and spatial patterns from satellite observations, Journal of Marine Systems, 37,
999   69-86, 2002.

1000 Müller, J., Wagner, A., Fahl, K., Stein, R., Prange, M., and Lohmann, G.: Towards quantitative sea
1001   ice reconstructions in the northern North Atlantic: A combined biomarker and numerical
1002   modelling approach, Earth and Planetary Science Letters, 306, 137-148, 2011.

1003 Müller, J., and Stein, R.: High-resolution record of late glacial and deglacial sea ice changes in Fram
1004   Strait corroborates ice–ocean interactions during abrupt climate shifts, Earth and Planetary
1005   Science Letters, 403, 446-455, 2014.

Nakayama, Y., Schröder, M., Hellmer, H.H.: From circumpolar deep water to the glacial meltwater plume on the eastern Amundsen Shelf. Deep Sea Research Part I: Oceanographic Research Papers 77, 50-62, 2013.

Nakayama, Y., Menemenlis, D., Zhang, H., Schodlok, M. and Rignot, E.: Origin of Circumpolar Deep Water intruding onto the Amundsen and Bellingshausen Sea continental shelves. Nature Communications 9, 3403, 2018.

Nicholls, K. W., Østerhus, S., Makinson, K., Gammelsrød, T., and Fahrbach, E.: Ice-ocean processes over the continental shelf of the southern Weddell Sea, Antarctica: A review, Reviews of Geophysics, 47, https://doi.org/10.1029/2007RG000250, 2009.

Nichols, P. D., Palmisano, A. C., Volkman, J. K., Smith, G. A., and White, D. C.: Occurrence of an isoprenoid C_{25} diunasaturated alkene and high neutral lipid content in Antarctic sea-ice diatom communities 1, Journal of Phycology, 24, 90-96, 1988.

Nielsdóttir, M. C., Bibby, T. S., Moore, C. M., Hinz, D. J., Sanders, R., Whitehouse, M., Korb, R., and Achterberg, E. P.: Seasonal and spatial dynamics of iron availability in the Scotia Sea, Marine Chemistry, 130, 62-72, 2012.

Nolting, R., De Baar, H., Van Bennekom, A., and Masson, A.: Cadmium, copper and iron in the Scotia Sea, Weddell Sea and Weddell/Scotia confluence (Antarctica), Marine Chemistry, 35, 219-243, 1991.

Orsi, A. H., Whitworth III, T., and Nowlin Jr, W. D.: On the meridional extent and fronts of the Antarctic Circumpolar Current, Deep Sea Research Part I: Oceanographic Research Papers, 42, 641-673, 1995.

Otto-Bliesner, B., Brady, E., Zhao, A., Brierley, C., Axford, Y., Capron, E., Govin, A., Hoffman, J., Isaacs, E., and Kageyama, M.: Large-scale features of Last Interglacial climate: Results from evaluating the lig127k simulations for CMIP6-PMIP4, Climate of the Past, 17, 63-94, 2021.

Otto-Bliesner, B. L., Braconnot, P., Harrison, S. P., Lunt, D. J., Abe-Ouchi, A., Albani, S., Bartlein, P. J., Capron, E., Carlson, A. E., and Dutton, A.: The PMIP4 contribution to CMIP6–Part 2: Two interglacials, scientific objective and experimental design for Holocene and Last Interglacial simulations, Geoscientific Model Development, 10, 3979-4003, 2017.

Park, E., Hefter, J., Fischer, G., Iversen, M. H., Ramondenc, S., Nöthig, E.-M., and Mollenhauer, G.: Seasonality of archaeal lipid flux and GDGT-based thermometry in sinking particles of high-latitude oceans: Fram Strait (79° N) and Antarctic Polar Front (50° S), Biogeosciences, 16, 2247-2268, 2019.

Parkinson, C. L., and Cavalieri, D. J.: Antarctic sea ice variability and trends, 1979-2010, The Cryosphere, 6, 871-880, 2012.

Parkinson, C. L.: A 40-y record reveals gradual Antarctic sea ice increases followed by decreases at rates far exceeding the rates seen in the Arctic, Proceedings of the National Academy of Sciences, 116, 14414-14423, 2019.

Paul, S., Willmes, S., and Heinemann, G.: Long-term coastal-polynya dynamics in the southern Weddell Sea from MODIS thermal-infrared imagery, The Cryosphere, 9, 2027-2041, 2015.

Pritchard, H., Ligtenberg, S., Fricker, H., Vaughan, D., Van den Broeke, M., and Padman, L.: Antarctic ice-sheet loss driven by basal melting of ice shelves, Nature, 484, 502-505, 2012.

Raddatz, T., Reick, C., Knorr, W., Kattge, J., Roeckner, E., Schnur, R., Schnitzler, K.-G., Wetzel, P., and Jungclaus, J.: Will the tropical land biosphere dominate the climate–carbon cycle feedback during the twenty-first century?, Climate dynamics, 29, 565-574, 2007.

Riaux-Gobin, C., and Poulin, M.: Possible symbiosis of Berkeleya adeliensis Medlin, Synedropsis fragilis (Manguin) Hasle et al. and Nitzschia lecointei Van Heurck (Bacillariophyta) associated with land-fast ice in Adélie Land, Antarctica, Diatom Research, 19, 265-274, 2004.

Riaux-Gobin, C., Dieckmann, G. S., Poulin, M., Neveux, J., Labrune, C., and Vetion, G.: Environmental conditions, particle flux and sympagic microalgal succession in spring before the sea-ice break-up in Adélie Land, East Antarctica, Polar Research, 32, https://doi.org/10.3402/polar.v32i0.19675, 2013.

Rignot, E., Mouginot, J., Scheuchl, B., Van Den Broeke, M., Van Wessem, M.J., Morlighem, M.: Four decades of Antarctic Ice Sheet mass balance from 1979–2017. Proceedings of the National Academy of Sciences 116, 1095-1103, 2019.

Rintoul, S., Hughes, C., and Olbers, D.: The Antarctic circumpolar current system, International Geophysics, 77, 271-302, 2001.

1062 Roeckner, E., Dümenil, L., Kirk, E., Lunkeit, F., Ponater, M., Rockel, B., Sausen, R., and Schlese,

1063   U.: The Hamburg version of the ECMWF model (ECHAM), Research activities in atmospheric

1064   and oceanic modelling. CAS/JSC Working Group on Numerical Experimentation, 13, 7.1-7.4,

1065   1989.

1066 Rontani, J.-F., Belt, S.T. and Amiraux, R.: Biotic and abiotic degradation of the sea ice diatom

1067   biomarker IP$_{25}$ and selected algal sterols in near-surface Arctic sediments, Organic Geochemistry

1068   118, 73-88, 2018.

1069 Rontani, J.-F., Smik, L. and Belt, S.T.: Autoxidation of the sea ice biomarker proxy IPSO$_{25}$ in the

1070   near-surface oxic layers of Arctic and Antarctic sediments, Organic Geochemistry 129, 63-76,

1071   2019.

1072 Sangrà, P., Gordo, C., Hernández-Arencibia, M., Marrero-Díaz, A., Rodríguez-Santana, A., Stegner,

1073   A., Martínez-Marrero, A., Pelegrí, J. L., and Pichon, T.: The Bransfield current system, Deep Sea

1074   Research Part I: Oceanographic Research Papers, 58, 390-402, 2011.

1075 Scambos, T. A., Bell, R. E., Alley, R. B., Anandakrishnan, S., Bromwich, D., Brunt, K.,

1076   Christianson, K., Creyts, T., Das, S., and DeConto, R.: How much, how fast?: A science review

1077   and outlook for research on the instability of Antarctica's Thwaites Glacier in the 21st century,

1078   Global and Planetary Change, 153, 16-34, 2017.

1079 Schmidt, K., Brown, T. A., Belt, S. T., Ireland, L. C., Taylor, K. W., Thorpe, S. E., Ward, P., and

1080   Atkinson, A.: Do pelagic grazers benefit from sea ice? Insights from the Antarctic sea ice proxy

1081   IPSO$_{25}$, 15, 1987-2006, 2018.

1082 Schmidtko, S., Heywood, K. J., Thompson, A. F., and Aoki, S.: Multidecadal warming of Antarctic

1083   waters, Science, 346, 1227-1231, 2014.

1084 Schofield, O., Brown, M., Kohut, J., Nardelli, S., Saba, G., Waite, N., and Ducklow, H.: Changes in

1085   the upper ocean mixed layer and phytoplankton productivity along the West Antarctic Peninsula,

1086   Philosophical Transactions of the Royal Society A: Mathematical, Physical and Engineering

1087   Sciences, 376, https://doi.org/10.1098/rsta.2017.0173, 2018.

1088 Schouten, S., Hopmans, E. C., Schefuß, E., and Sinninghe Damsté, J. S.: Distributional variations in

1089   marine crenarchaeotal membrane lipids: a new tool for reconstructing ancient sea water

1090   temperatures?, Earth and Planetary Science Letters, 204, 265-274, 2002.

1091 Schouten, S., Hopmans, E. C., and Sinninghe Damsté, J. S.: The organic geochemistry of glycerol

1092   dialkyl glycerol tetraether lipids: A review, Organic Geochemistry, 54, 19-61, 2013.

1093 Schröder, M.: The Expedition PS111 of the Research POLARSTERN to the southern Weddell Sea

1094   in 2018, Berichte zur Polar-und Meeresforschung = Reports on polar and marine research, 718,

1095   2018.

1096 Sidorenko, D., Goessling, H., Koldunov, N., Scholz, P., Danilov, S., Barbi, D., Cabos, W., Gurses,

1097   O., Harig, S., and Hinrichs, C.: Evaluation of FESOM2. 0 coupled to ECHAM6. 3: Preindustrial

1098   and HighResMIP simulations, Journal of Advances in Modeling Earth Systems, 11, 3794-3815,

1099   2019.

1100 Smik, L., Belt, S. T., Lieser, J. L., Armand, L. K., and Leventer, A.: Distributions of highly branched

1101   isoprenoid alkenes and other algal lipids in surface waters from East Antarctica: further insights

1102   for biomarker-based paleo sea-ice reconstruction, Organic Geochemistry, 95, 71-80, 2016.

1103 Smith, J.A., Hillenbrand, C.-D., Kuhn, G., Larter, R.D., Graham, A.G.C., Ehrmann, W., Moreton,

1104   S.G., Forwick, M.: Deglacial history of the West Antarctic Ice Sheet in the western Amundsen

1105   Sea Embayment, Quaternary Science Reviews 30, 488-505, 2011.

1106 Smith, J.A., Hillenbrand, C.-D., Kuhn, G., Klages, J.P., Graham, A.G.C., Larter, R.D., Ehrmann,

1107   W., Moreton, S.G., Wiers, S., Frederichs, T.: New constraints on the timing of West Antarctic

1108   Ice Sheet retreat in the eastern Amundsen Sea since the Last Glacial Maximum. Glob. Planet.

1109   Change 112, 224-237, 2014.

1110 Smith, J.A., Andersen, T., Shortt, M., Gaffney, A., Truffer, M., Stanton, T.P., Bindschadler, R.,

1111   Dutrieux, P., Jenkins, A., Hillenbrand, C.-D.: Sub-ice-shelf sediments record history of twentieth-

1112   century retreat of Pine Island Glacier, Nature 541, 77-80, 2017.

1113 Spencer-Jones, C. L., McClymont, E. L., Bale, N. J., Hopmans, E. C., Schouten, S., Müller, J.,

1114   Abrahamsen, E. P., Allen, C., Bickert, T., Hillenbrand, C. D., Mawbey, E., Peck, V., Svalova,

1115   A., and Smith, J. A.: Archaeal Intact Polar Lipids in Polar Waters: A Comparison Between the

Amundsen and Scotia Seas, Biogeosciences18, 3485-3504, https://doi.org/10.5194/bg-18-3485-2021, 2021.

Stevens, B., Giorgetta, M., Esch, M., Mauritsen, T., Crueger, T., Rast, S., Salzmann, M., Schmidt, H., Bader, J., and Block, K.: Atmospheric component of the MPI-M Earth system model: ECHAM6, Journal of Advances in Modeling Earth Systems, 5, 146-172, 2013.

Stocker, T. F., Qin, D., Plattner, G.-K., Tignor, M., Allen, S. K., Boschung, J., Nauels, A., Xia, Y., Bex, V., and Midgley, P. M.: The physical science basis. Contribution of working group I to the fifth assessment report of the intergovernmental panel on climate change, Computational Geometry, 18, 95-123, 2013.

Tesi, T., Belt, S., Gariboldi, K., Muschitiello, F., Smik, L., Finocchiaro, F., Giglio, F., Colizza, E., Gazzurra, G., and Giordano, P.: Resolving sea ice dynamics in the north-western Ross Sea during the last 2.6 ka: From seasonal to millennial timescales, Quaternary Science Reviews, 237, http://dx.doi.org/10.1016/j.quascirev.2020.106299, 2020.

Thomas, D. N.: Sea ice, John Wiley & Sons, 2017.

Thompson, A. F., Heywood, K. J., Thorpe, S. E., Renner, A. H., and Trasviña, A.: Surface circulation at the tip of the Antarctic Peninsula from drifters, Journal of Physical Oceanography, 39, 3-26, 2009.

Thompson, A. F., Stewart, A. L., Spence, P., and Heywood, K. J.: The Antarctic Slope Current in a changing climate, Reviews of Geophysics, 56, 741-770, 2018.

Turner, J., Orr, A., Gudmundsson, G. H., Jenkins, A., Bingham, R. G., Hillenbrand, C.-D., and Bracegirdle, T. J.: Atmosphere-ocean-ice interactions in the Amundsen Sea Embayment, West Antarctica, Reviews of Geophysics, 55, 235-276, 2017.

Turner, J., Guarino, M.V., Arnatt, J., Jena, B., Marshall, G.J., Phillips, T., Bajish, C.C., Clem, K., Wang, Z., Andersson, T., Murphy, E.J., Cavanagh, R.: Recent Decrease of Summer Sea Ice in the Weddell Sea, Antarctica, Geophysical Research Letters 47, e2020GL087127, 2020.

Valcke, S.: The OASIS3 coupler: A European climate modelling community software, Geoscientific Model Development, 6, 373-388, 2013.

Vaughan, D. G., Marshall, G. J., Connolley, W. M., Parkinson, C., Mulvaney, R., Hodgson, D. A., King, J. C., Pudsey, C. J., and Turner, J.: Recent rapid regional climate warming on the Antarctic Peninsula, Climatic change, 60, 243-274, 2003.

Vaughan, D. G.: West Antarctic Ice Sheet collapse–the fall and rise of a paradigm, Climatic Change, 91, 65-79, 2008.

Vernet, M., Geibert, W., Hoppema, M., Brown, P. J., Haas, C., Hellmer, H., Jokat, W., Jullion, L., Mazloff, M., and Bakker, D.: The Weddell Gyre, Southern Ocean: present knowledge and future challenges, Reviews of Geophysics, 57, 623-708, 2019.

Volkman, J. K.: Lipid markers for marine organic matter, in: Marine organic matter: Biomarkers, isotopes and DNA, Springer, 27-70, 2006.

Vorrath, M.-E., Müller, J., Esper, O., Mollenhauer, G., Haas, C., Schefuß, E., and Fahl, K.: Highly branched isoprenoids for Southern Ocean sea ice reconstructions: a pilot study from the WAP, Biogeosciences, 16, 2961-2981, 2019.

Vorrath, M.-E., Müller, J., Rebolledo, L., Cárdenas, P., Shi, X., Esper, O., Opel, T., Geibert, W., Muñoz, P., and Haas, C.: Sea ice dynamics in the Bransfield Strait, Antarctic Peninsula, during the past 240 years: a multi-proxy intercomparison study, Climate of the Past, 16, 2459-2483, 2020.

Wang, Z., Turner, J., Wu, Y., Liu, C.: Rapid Decline of Total Antarctic Sea Ice Extent during 2014–16 Controlled by Wind-Driven Sea Ice Drift. Journal of Climate 32, 5381-5395, 2019.

Witus, A.E., Branecky, C.M., Anderson, J.B., Szczuciński, W., Schroeder, D.M., Blankenship, D.D., Jakobsson, M.: Meltwater intensive glacial retreat in polar environments and investigation of associated sediments: example from Pine Island Bay, West Antarctica, Quaternary Science Reviews, 85, 99–118, 2014.

Xiao, X., Fahl, K., Müller, J., and Stein, R.: Sea-ice distribution in the modern Arctic Ocean: Biomarker records from trans-Arctic Ocean surface sediments, Geochimica et Cosmochimica Acta, 155, 16-29, 2015.

1169   Zamelczyk, K., Rasmussen, T. L., Husum, K., Haflidason, H., de Vernal, A., Ravna, E. K., Hald,

1170   M., and Hillaire-Marcel, C.: Paleoceanographic changes and calcium carbonate dissolution in the

1171   central Fram Strait during the last 20 ka, Quaternary Research, 78, 405-416, 2012.

1172   Zielinski, U., Gersonde, R., Sieger, R., and Fütterer, D.: Quaternary surface water temperature

1173   estimations: Calibration of a diatom transfer function for the Southern Ocean, Paleoceanography

1174   and Paleoclimatology, 13, 365-383, 1998.

1175   Zwally, H. J.: Antarctic sea ice, 1973-1976: Satellite passive-microwave observations, Scientific and

1176   Technical Information Branch, National Aeronautics and Space, 1983.

1177

1178